Title	非酸化物系セラミックスの高圧焼結
Author(s)	鷹取, 一雅
Citation	大阪大学, 1981, 博士論文
Version Type	VoR
URL	https://hdl.handle.net/11094/1451
rights	
Note	

HIGH PRESSURE SINTERING OF NON-OXIDE CERAMICS

Kazumasa TAKATORI

OSAKA UNIVERSITY
OSAKA, JAPAN
JANUARY, 1981

HIGH PRESSURE SINTERING OF NON-OXIDE CERAMICS

（非酸化物系セラミックスの高圧焼結）

Kazumasa TAKATORI

CONTENTS

Introduction

Ceramics based on non-oxide compounds such as silicon nitride (Si_3N_4), silicon carbide (SiC) and aluminum nitride (AlN) have received a considerable attention because of their possible utilization to the high temperature structural materials.[1-3]

Since the introduction of the gas turbine engine in the late 1930's, a great deal of efforts have been made by gas turbine engineers to achieve greater efficiency of energy conversion from heat to mechanical power. As a result, the efficiency of energy conversion has been developed up to about 40% in case when the superalloy was used as the present gas turbine engine material, and seems to have attained the end-point efficiency. There remains, however, the most valuable and most principal proble, that is, the development of the high temperature structural materials for gas turbien engine component. It is well known that higher operation temperature produces greater efficiency of the engine. To answer this demand, various high temperature superalloys have been improved up to the present by matallurgists, but these superalloys cannot be used at 1250°C - 1400°C that is required today for the operation temperature of the advanced gas turbine engine. Thus the development of the high temperature materials has been required.

Recently the ceramics have been expected[4,5] as the

materials to solve the above-mentioned problem. They formerly could not be accepted for the high strength structural materials because of their brittle character. However some of the new ceramics such as Si_3N_4, SiC and AlN have become clear to exhibit high mechanical strength and chemical stability up to elevated temperatures. These non-oxide ceramics are so-called high performance ceramics and expected to be used for the high temperature-high strength materials in near future. The non-oxide ceramics show special characters due to their dominance in bond nature of covalency[6] differing from oxide with ionic bonding. Table 1 shows the comparison of general characters of non-oxides, oxides and metals.

The strucural materials of ceramic are generally produced by sintering. Most of the oxide ceramics can be easily fabricated by normal sintering. On the other hand, it is very difficult to sinter non-oxide ceramics with a mechanical strength enough to use for the mechanical devices. Since the driving force in densification is only the difference between surface energy and grain boundary energy in case of normal sintering,[7-11] the well self-bounded and dense sintered non-oxides ceramics cannot be obtained by normal sintering owing to their covalent bond character. It is well known that the mechanical strength of sintered material strongly depends on the porosity.[12] Well self-bonded and dense sintered bodies are required for high mechanical strength materials. In order to get a fully dense ceramic without pore, the hot-pressing technique at 10 MPa has been developed in the fabrication

Table 1 General comparison of characters for non-oxides, oxides and metals

Characters	Non-oxides	Oxides	Metals
Dominant bonding nature	covalent	ionic	metallic
Specific weight	small	small	large
Melting point	high	high	low
Thermal expansion	small	small	large
Thermal shock resistance	good	bad	bad
Fracture nature	catastrophic	catastrophic	yield
Machinability	bad	bad	good

of non-oxide ceramics with some amounts of oxide additives such as MgO,[13-18] Y_2O_3[19-21] and Al_2O_3.[22,23] The fully dense materials with high strength at room temperature have been fabricated by this method. The above oxide additives react with non-oxide material in the sintering process and glassy secondary phases precipitates at grain boundaries. A problem, however, still remains. Although hot-pressed non-oxide ceramics with additives keep their high strength up to 800 - 1000°C, drastic fall-down in mechanical strength due to the existence of secondary phases occurs at higher temperatures[24] (Fig. 1). Many efforts are put into the research of new additives which improves the high temperature strength.[25-29] Another research to solve the problem is the development of new sintering techniques. The consolidation of pure phase of non-oxide material into self-bonded and dense bodies is so difficult that there are few research on sintering of non-oxides without any additives.[30-35]

In the present study, non-oxide ceramics were sintered without any additives by applying high pressure technique with respect to the following object; One purpose is to make clear the sintering mechanism of the covalent material under pressure. Another is to fabricate the highly pure and dense non-oxide ceramics with high mechanical strenth at elevated temperature. Three kinds of materials such as silicon (Si), titanium carbide (TiC) and Si_3N_4 were selected to attain these purposes.

This thesis describes the sintering mechanism of covalent materials under high pressures and the micro-
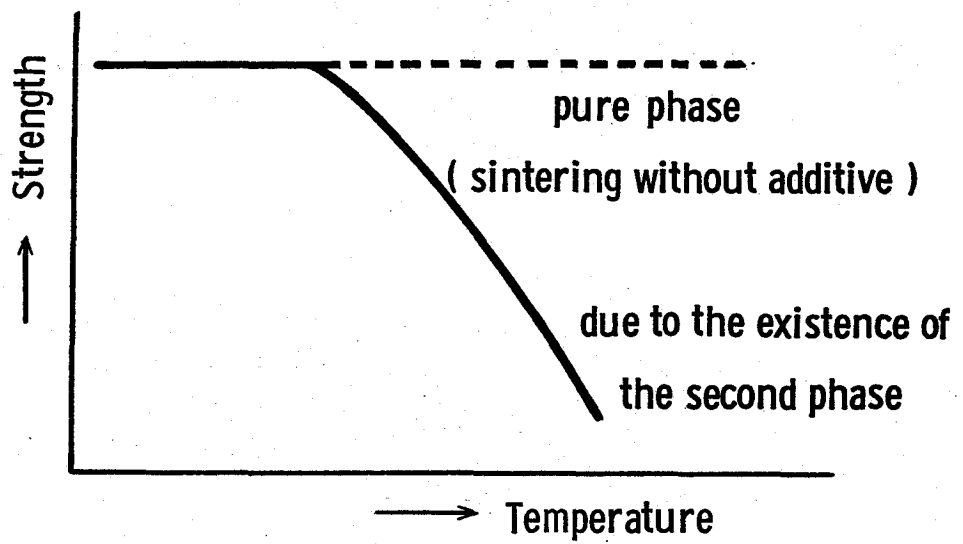
Fig. 1 Scheme of mechanical strength versus
temperature curve for sintered non-oxide ceramics.

hardness of highly pure and dense sintered material at high temperatures.

It is constructed by seven chapters. The content of each chapter is as follows.

Chapter I presents the experimental procedure and various apparatus used in high pressure sintering and methods of characterization for fabricated specimens.

In Chapter II, various factors affecting the densification mechanism in high pressure sintering is discussed.

In Chapter III, diffusion coefficients of carbon in TiC under quasihydrostatic high pressure are investigated and self-bonding between particles is discussed. At the end of the chapter the sintering mechanism in high pressure sintering is summarized in general.

Chapter IV presents the consolidation process of Si_3N_4. In case of Si_3N_4, special factor of phase transformation is also discussed in sintering mechanism.

In Chapter V, mechanical and thermal properties of high pressure sinterd TiC and Si_3N_4 are reported. Temperature dependences of both properties of the present specimens are compared with those reported in literatures.

The results revealed in this study are presented in Summary.

Chapter I

Experimental

I - 1   Experimental Procedure

The experimental procedure of high pressure sintering and the characterization of sintered bodies are schematically shown in Fig. I-1. Commercial-grade powders were used as starting materials. As for the present high pressure sintering experiments, the pressure, temperature and sintering time conditions were 5.0 GPa, 1800°C and 200 minutes in maximum, respectively. Runs of high pressure sitnering were carried out as mentioned below. At first pressure was applied at room temperature. And then, temperature was raised rapidly to a desired condition, and specimen was held at the high pressure-temperature condition for a desired duration. Then, the specimen was quenched to room temperature, and pressure was released. The sintered material was withdrawn and supplied to various measurements. To characterize the sitnered specimen, bulk density, microstructure and crystalline phase were examined. As for mechanical and thermal properties of the specimens, the temperature dependence of Vickers micro-hardness and thermal diffusivity of sintered TiC and Si_3N_4 were measured.

I - 2   High Pressure Apparatus

The experiments of high pressure sintering were conducted by using three different types of high pressure

EXPERIMENTAL PROCEDURE

Starting powders

High pressure
sintering

up to $\left\{\begin{array}{l} 5.0 \text{ G Pa} \\ 1800 °C \\ 200 \text{ min} \end{array}\right.$

Sintered bodies

Water displacement
method

Indentation method
R.T. — 1200°C

Density

Vickers
microhardness

SEM

Microstructure

Laser pulse method
R.T. — 850°C

X-ray diffractometry
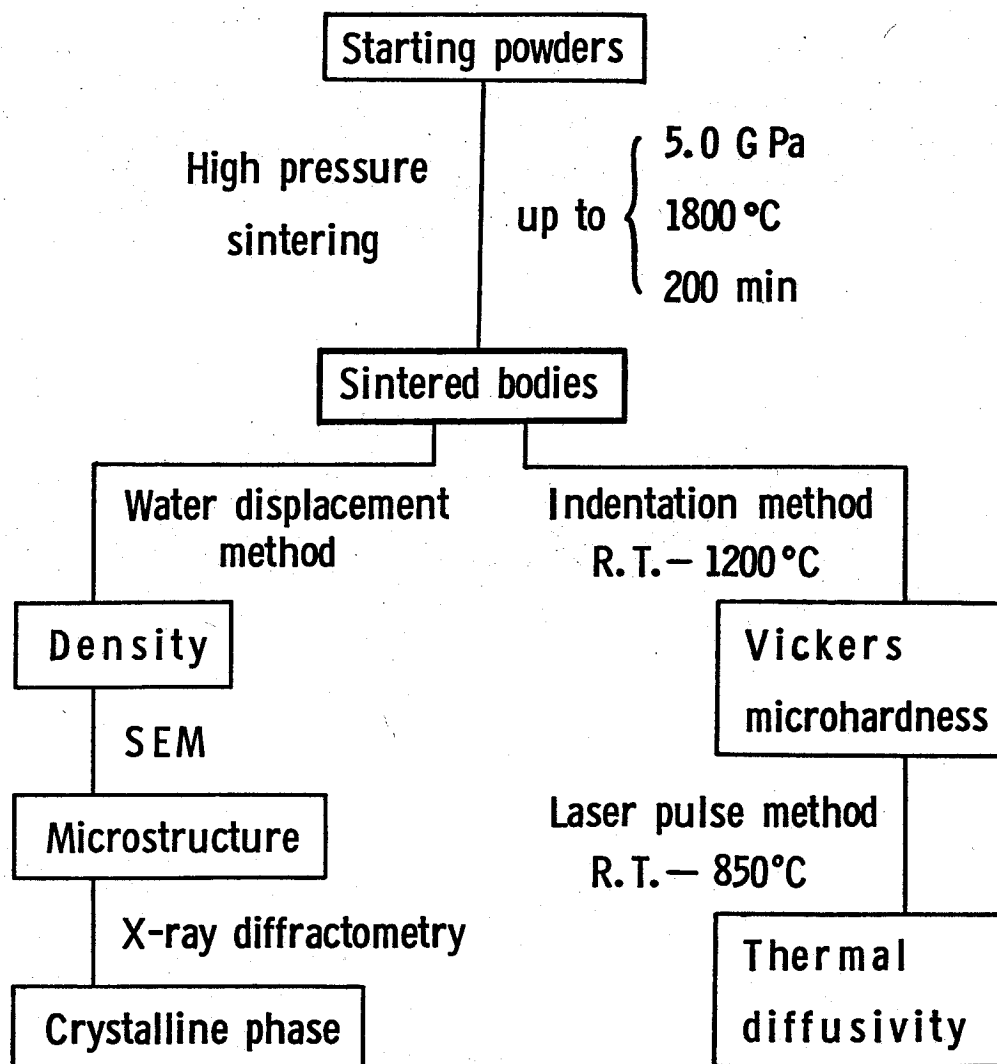
Crystalline phase

Thermal
diffusivity

Fig. I-1   Schematic diagram of experimental procedure.

apparatus such as a a cubic anvil type, a piston cylinder type and a hot isostatic type according to the magnitude and hydrostaticity of pressure. Characteristics of high pressure apparatus mentioned above are listed in Table I-1.

In the pressure range from 1.0 to 5.0 GPa, cubic anvil type and poston cylinder type high pressure apparatus were operated, in which pyrophyllite was used as pressure medium. The magnitude of pressure generated inside the high pressure cell was calibrated at room temperature by the change of the electrical resistivity in bismuth I - II and barium I- II transitions at 2.55 and 5.5 GPa, respectively. Heating of the sample was carried out by Joule heating of graphite heater, and temperature was monitored with Pt/Pt-13%Rh or Pt-20%Rh/Pt-40%Rh thermocouple inserted in the cell. The starting powders were compressed to the form of pellet 5^{ϕ}x 2.5^{t}mm at room temperature. The powder compacts were put into BN containers and charged into a high pressure cell assembly.

In the pressure range less than 100 MPa, hot isostatic pressing (HIP) was conducted. The pelletized sample was put into BN capsule which was placed in a container made of Pyrex glass. The Pyrex container was evacuated to less than 1 Pa, and then sealed off. The glass-cealed specimen was placed into the hot zone of a high pressure vessel, and HIP experiments were performed using argon or nitrogen gas as a pressure-transmitting medium. The specimen was heated to the softening point of Pyrex glass under a pressure of 20 MPa, and then pressure and temperature were simultaneously raised to desired conditions.

Table I-1   High pressure apparatus

alias	pressure medium	sample size(mm^3)	maximum pressure (MPa)	maximum temperature (°C)
Cubic anvil type	solid	$5\phi \times 5^l$	7000	1900
Piston cylinder type	solid	$7\phi \times 8^l$	3000	1700
Hot isostatic pressing	gas	$15\phi \times 35^l$	200	2500

High temperature was generated by Joule heating of graphite heater or radio-frequency heating of graphite crucible. The temperature of the specimen placed inside the furnace was monitored with a Pt-6%Rh/Pt-30%Rh or W-3%Re/W-25%Re thermocouple.

I - 3   Characterization of Sintered Bodies

I - 3 - 1   Bulk Density Measurements

The bulk densities of the high pressure sintered specimens were measured by a liquid displacement technique using distilled water. Before measurements, enamel was coated on the specimens with open pores, whose densities were less than about 90% of theoretical density. The maximum error of this technique was estimated to be ±5% and ±0.5% for the specimens with and without coating of enamel in case when the dislocation-free single crystal of silicon as standard materials.

I - 3 - 2   Microstructure Observations

It is well knwon[36-39] that grain size, grain morphology and distribution of pores are very important factors to understand the mechanical behavior of sintered materials. In this study, gold-coated fractured surfaces and etched surfaces after polishing were observed by scanning electron microanalysis. The mixture of fluoric acid and nitric acid was used as the etchant for Si and TiC.

I - 3 - 3   Crystalline Phase Determinations

The crystalline phase and the weight fractions of phases of sintered body were determined by X-ray powder

diffractometry using Ni-filtered Cu Kα radiation.

No diffraction patterns of oxides were observed in either starting powders or sintered specimens.

The weight fractions of phases in the mixture of α- and β-Si_3N_4 were determined by the method of Gazzara and Messier[40] using diffraction peak heights of (210) of each phase.

I - 3 - 4   Vickers Microhardness Measurements

In order to characterize one of the mechanical strength, microhardness of the sinterd specimens was measured. The high pressure sintered specimens were polished with various grades of diamond paste to obtain mirror-like surfaces for measurements. Microhardness measurements were made by a high temperature microhard-ness tester[*] using a Vickers diamond indenter.

Vickers microhardness (DPN) is given by the relation:

$$H_v = 1854.4 \ P/d^2$$

where P is the load and d is the length of indentation diagonal. The relation between P and d can be expressed by the expirical Meyer equation[41]:

$$P = a \cdot d^n$$

where a and n are constants depending on the materials. Therefore, the relation between Vickers microhardness and the load can be obtained from the above two equations as follows:

---

*Nippon Kogaku K. K. Japan, QM type

$$H_v = 1854.4 \; a^{(\frac{2}{n})} \; P^{\; 1-(\frac{2}{n})}$$

The indentation loads in the range of 50 - 200 g were applied to the specimens for 5 seconds with loading rate of 80 $m \cdot sec^{-1}$, and the relation between the hardness and the load was determined. In the present experiments, the values for the Meyer exponent n of high pressure sintered bodies were 1.95 and the weight of load was experimentally determined to be 200 g so as not to originate cracks but to make as large indentations as possible. Microhardness at room temperature was measured in air, and temperature dependence of it in the temeprature range from room temperature to 1200°C was measured in high vacuum of less than 10 mPa. There was a remarkable effect of atmospheric conditions on microhardness probably caused by moisture.[42,43]

I - 3 - 5   Thermal Diffusivity Measurements

Thermal shock resistance at elevated temepratures is required for high temperature structural materials. Since one of the most important parameters to dominate the thermal shock resistance is thought to be the thermal diffusivity, in this study, the thermal diffusivity was measured by means of the laser pulse method[44] from room temperature to 850°C in high vacuum less than 10 mPa. The source of energy pulse was a ruby laser with 694.3 nm.* The specimens were polished into parallel flat disk. Front surface of the specimen was coated by dry carbon, on which a laser pulse was irradiated. To monitor the temperature response

---

* Sinku Riko K. K. Japan, TC 3000 type

of the back surface, the Pt/Pt-13%Rh thermocouple was used. The construction of the specimen and the time dependence of temeprature rise on the back surface are schematically shown in Fig. I-2. The thermal diffusivity α is given by;

$$\alpha = \frac{1.38}{\pi^2} \times \frac{\ell^2}{t_{1/2}} \quad (cm^2 sec^{-1})$$

where ℓ is the sample thickness in cm and $t_{1/2}$ is a half time (sec) designated in Fig. I-2. The calibration was carried out by stainless steel 304 and sapphire as standard materials.
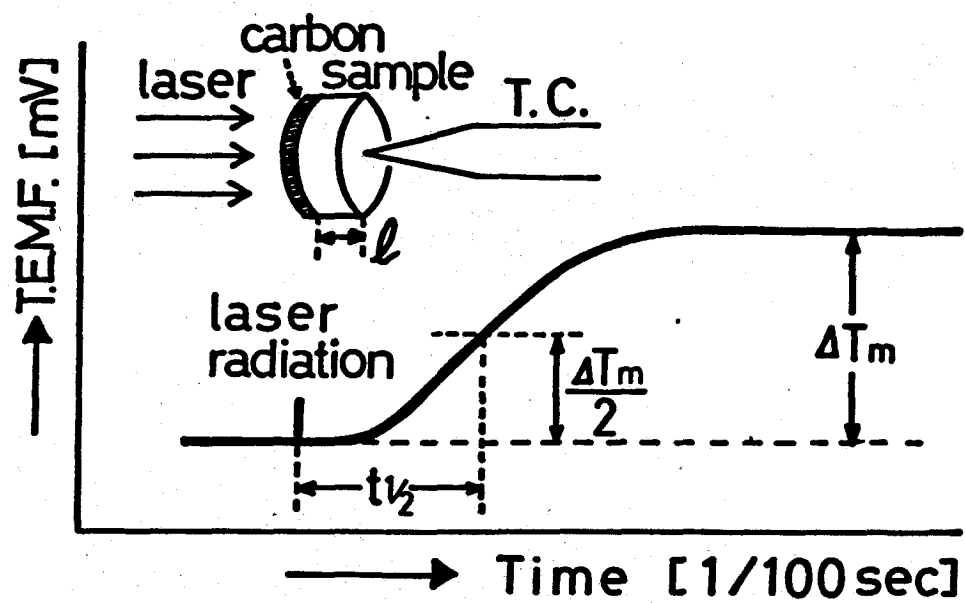
Fig. I-2 Construction of specimen and back surface temperature history in laser pulse method.

Chapter II

Densification Mechanism under High Pressure

II - 1   Introduction

It is well known that the chemical bond nature of non-oxide materials is covalent. The physical and chemical properties such as high hardness, high mechanical strength, superior oxidation and thermal shock resistances of non-oxide materials are closely related to its bond nature of covalent bonding. The consolidation of pure non-oxides into dense self-bonded ceramics without additives is very difficult by means of the normal sintering or conventional hot-pressing method due to the strong covalent nature. Although it is expected that high pressure sintering is one of the most useful sintering techniques to consolidate the strong covalent bonding material into the dense ceramics without additives, there are few reports on sintering mechanism under high pressure of pure non-oxide materials.[30-35] Therefore, study on sintering mechanism of the strong covalent bonding materials under high pressure is not only very interesting from the view-point of basic science but also practically very important for the fabrication of non-oxide materials in industry. This chapter is devoted to make clear the densification mechanism under pressure, which takes place prior to the diffusion dominant stage. For this purpose, Si and TiC were used as model materials.

Si is a representative material with covalent bonding

and its physical and chemical properties[45] have been fully defined to apply for the electronic devices. Some of those are shown in Table II-1. The pressure dependence of the melting point of Si was reported by Babb, Jr.[46] According to his results, the melting point decreased about 58°C by application of pressure of 1.0 GPa. The diffusion coefficients were about 10^{-15} and 10^{-13} $cm^2 sec^{-1}$ at 1090°C and 1250°C,[47] respectively.

TiC is one of the non-oxide compounds, whose electrical and thermal conductivities are characterized by the electron conduction.[48,49] As TiC is easily synthesized, many investigations have been reported on its properties of both single crystal and polycrystal. At present, TiC is practically used mainly as a cermet for cutting tools.

As for sintering, it is generally said that the densification behavior and final density are strongly influenced by many factors such as characteristics of starting powders and sintering conditions as listed in Table II-2. In this chapter, the effects of particle size of starting powders and of principal variables such as temperature, pressure and sintering time on densification of Si and TiC powders in pressure sintering are investigated in detail. At the end of this chapter, the densification mechanism in high pressure sintering is discussed.

II - 2   High Pressure Sintering of Silicon Powders

Three different kinds of powders* were used as the

---

* Kojundo Kagaku Kenkyusho Co. Ltd., Japan

Table II-1   Characteristics of silicon

Crystal structure	Diamond type
Density	2.33 $(g \cdot cm^{-3})$
Melting point	$1685 - \dfrac{P}{1.72 \times 10^{7}}$ (K), P: (Pa)
Diffusion constant	$9000 \exp(-5.13eV/kT)$ $(cm^{2}sec^{-1})$

Table II-2 Some factors of sintering

Starting powder	$\left\{\begin{array}{l}\text{particle size}\\\text{particle shape}\\\text{crystalline phase}\\\text{impurity}\end{array}\right.$
Sintering condition	$\left\{\begin{array}{l}\text{temperature}\\\text{duration}\\\text{pressure}\\\text{atmosphere}\\\text{heating rate}\end{array}\right.$

starting powder. The average particle sizes were calculated from the values of specific surface areas measured by BET method using argon gas; 2.1 μm (purity 99.99%), 0.88 μm (99.9%) and 0.056 μm (99.9%). The temperature dependences of the relative density for the specimens obtained by the sintering of these powders at 3.0 GP for 4 minutes are shown in Fig. II-1. Temperatures are normalized by the melting point of Si at 3.0 Pa, and 0.17 T_m corresponds to room temperature. When the powders of 0.056 μm were used as the starting material, the green density and the relative density were the lowest among the bodies from different powders sintered at temepratures lower than $0.5T_m$. In case when the powders were sintered at the temperature range above $0.7T_m$, however, there was no difference in the relative densities of the products.

Using 2.1 and 0.88 μm powders as the starting materials, the effect of isothermal sintering time on the relative density was investigated under the conditions in which dense sintered bodies were obtained. The results are shown in Table II-3. In this table, flash means a subsequent quenching after reaching the desired temperature. As seen in Table II-3, there are no time dependences of densities under the present high pressure sintering conditions. In the present experiments, the specimens were heated to the desired temperature within 9 seconds and quenched to room temperature within 6 seconds. Considering these conditions and results listed in Table II-3, it is expected that the densification of Si occurred during heating time up to the desired temperature.
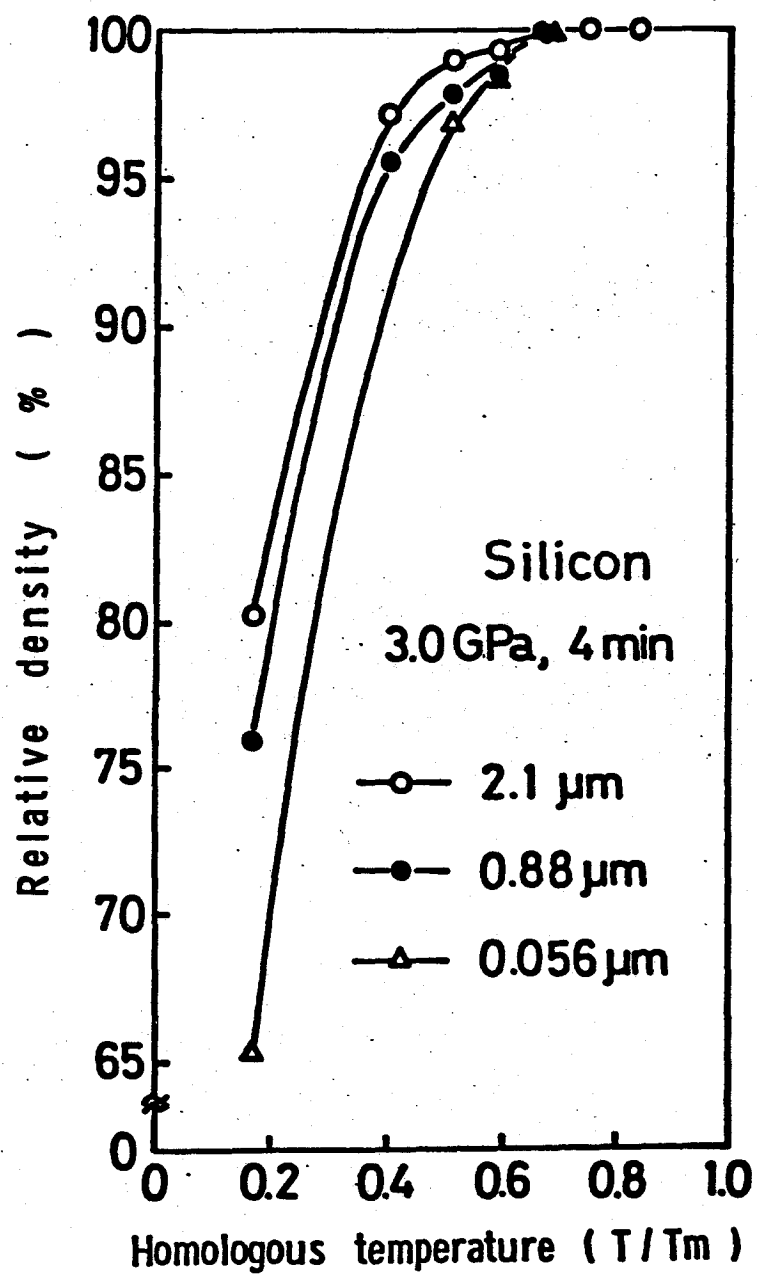
Fig. II-1   Relative density vs homologous temperature of high pressure sintered compacts at 3.0 GPa for 4 minutes using three kinds of powders.

Table II-3 Time dependence of the relative density of Si bodies sintered at 3.0 GPa using two kinds of starting powders

Sintering duration	2.1 μm^ϕ 0.59T_m	2.1 μm^ϕ 0.84T_m	0.88 μm^ϕ 0.59T_m
Flash	99.2	99.9	98.9
15 sec	99.1	100	99.0
30 sec	99.2	100	98.5
1 min	99.4	100	99.3
2 min	99.4	100	99.4
4 min	99.3	100	99.2

Mean error of the relative density is within ±0.5 %.

Fig. II-2 shows a temperature dependence of density of Si at different magnitudes of applied pressure. The powder of 2.1 μm particle size was used as the starting material. The temperatures are normalized by the melting point of Si at each magnitude of pressure. Fully dense sintered bodies were obtained at $0.6T_m$ above 3.0 GPa, but the relative density of the specimen sintered at $0.6T_m$ and 1.0 GPa was 92% of theoretical. At high temperature of $0.9T_m$, there were no differences in relative densities of the sintered bodies obtained by different magnitudes of applied pressure.

Using Si powder having 0.056 μm particle size, the pressure dependence of density was also investigated at the pressure range less than 1.0 GPa, and the results are shown in Fig. II-3. Comparing the results of densification of Si powders obtained by pressure sintering with those of pressure-less sintering, it is seen that Si powders were drastically densified at above $0.6T_m$ under the conditions of applied pressure, even if the magnitude of pressure was very small of 10 MPa. It is reported that the drastic densification at $0.6T_m$ under pressure is closely related to the transformation of the mechanical behavior of Si from brittle to ductile nature at high pressure-temperatures. Kohlstedt[50] measured the temperature dependences of Vickers microhardness of Si and TiC. The result is shown in Fig. II-4 (b). The microhardness of Si abruptly decreased at about 0.5 - $0.6T_m$, which corresponded to the brittle-ductile transition temperature of Si. Typical result of temperature
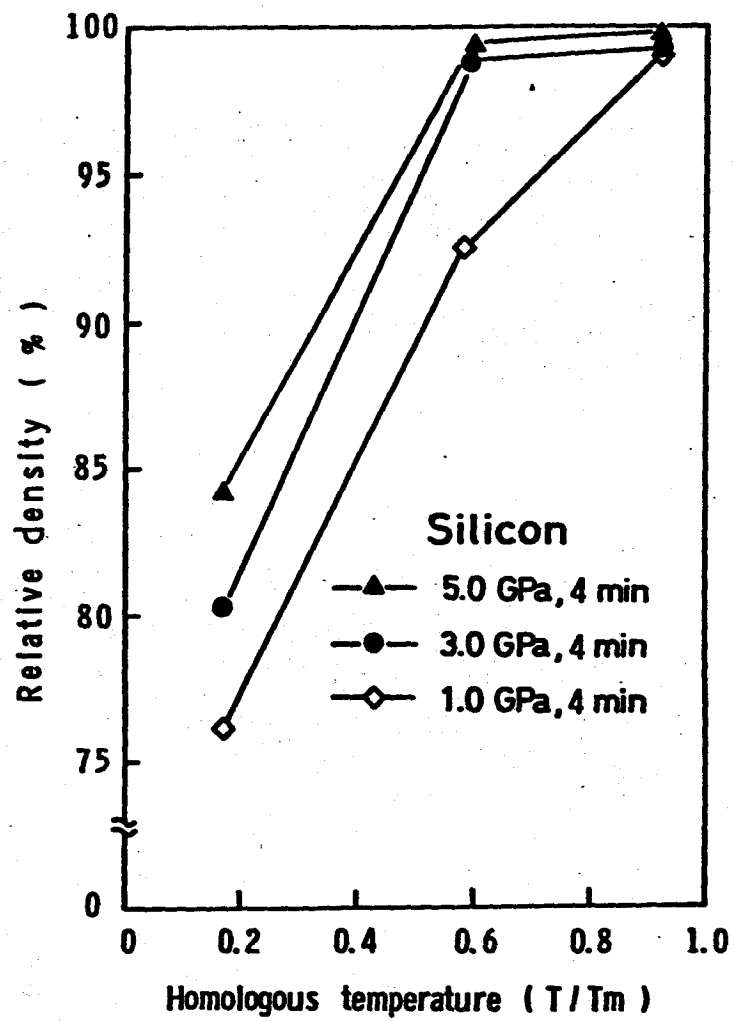
- 23 -

Fig. II-2 Relative density versus
homologous temperature of high pres-
sure sintered silicon compacts at
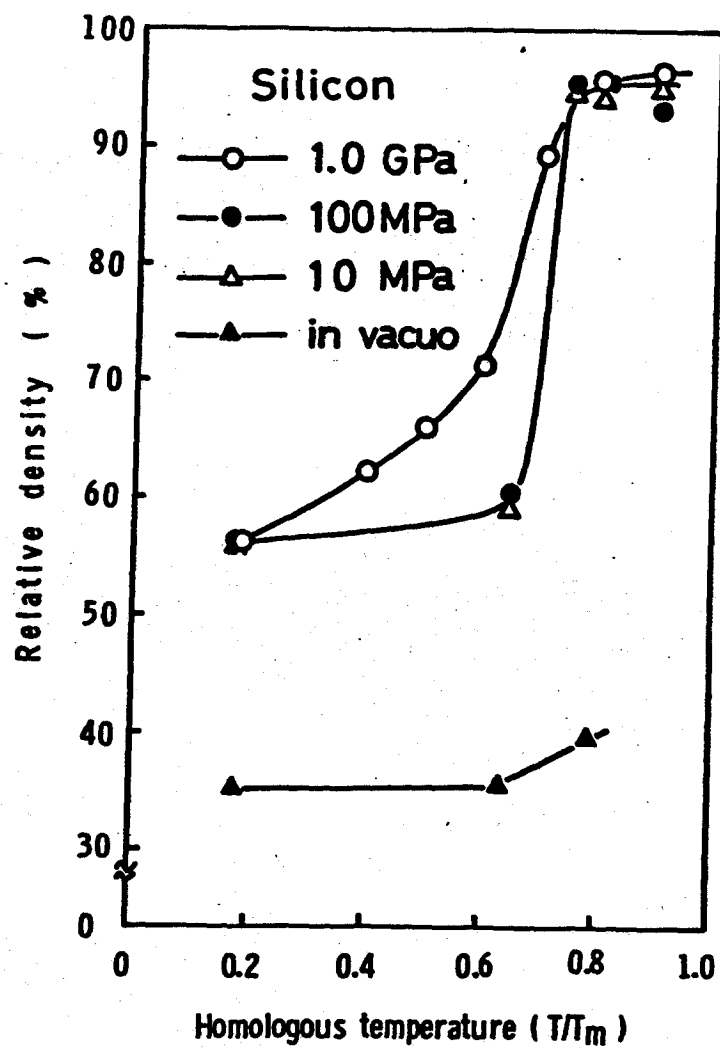5.0, 3.0 and 1.0 GPa for 4 minutes.

Fig. II-3 Relative density versus homologous temperature of high pressure sintered silicon compacts at various pressures.
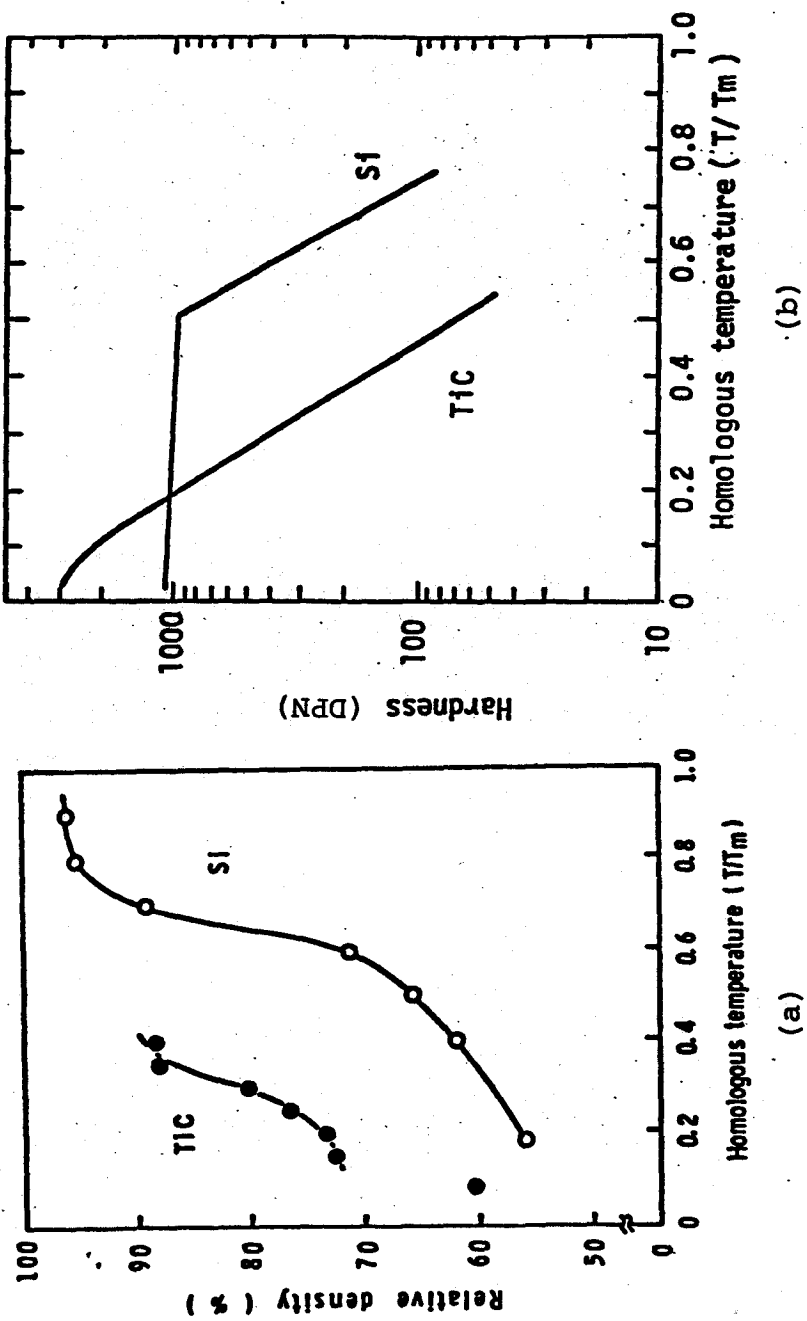
Fig. II-4   Temperature dependence of relative density (a) and of

Vickers microhardness[50] (b) for Si and TiC.

dependence of the relative density of sintered Si under pressuures is shown in Fig. II-4 (a). From the results of temperature dependence of microhardness of Si, it is expected that the rapid densification at $0.6T_m$ was due to the plastic deformation of Si corresponding to the brittle-ductile transition.

According to the relation between the mechanical toughness of a material and the effective stress of applied pressure, there are four cases in the effect of pressure on densification as listed below.

1)   In case when stress is much larger than toughness, the particles are crushed and the fully dense compacts are obtained without raising the temperature.

2)   When stress is nearly equal to toughness, the density gradually increases with increasing of the temperature due to the gradual decrease of material's toughness, and levels off below the transition temperature.

3)   In case when stress is smaller than toughness, the remarkable densification is observed at a temperature just above the brittle-ductile transition temperature.

4)   In pressure-less conditions, the driving force of densification is only the difference between surface energy and grain boundary energy, and the densification caused by diffusion mechanism markedly takes place just below the melting point.

The pressure-less sintering of Si was carried out by Greskovich and Rosolowski[30], and their results are presented in Table II-4, in which the present representative results are also listed. As seen in this table, it is

Table II-4 Comparison of results of the present work with those reported by Greskovich et al.[30]

	Present work	Greskovich et al.
Starting powder	coarse (2.1 μm^{ϕ})	fine (0.06 μm^{ϕ})
Pressure	1.0 GPa	0.1 MPa (in Ar)
Heating duration	4 min	60 min
Temperature	677°C 1218°C	1350°C 1350, 1400
Relative density	92.5 % 99.2 %	92 % 99 %

clear that fully dense sintered bodies can be obtained
at much lower temperatures and shorter sintering duration
in the present study.

Fig. II-5 shows the temperature dependence of micro-
structure of high pressure sintered specimens susing the
Si powders with a particle size of 0.88 μm as starting
material. The relative density of each specimen was
already shown in Fig. II-1. As seen in Fig. II-5, there
were considerably wide distribution in particle size and
some cracks were originated within large grains in the
green compact compressed at room temperature. The speci-
mens sintered below $0.59T_m$, whose microstructures are
shown in (b), (c) and (d) of this figure, showed similar
grain morphology each other and little self-bonding of
particles was observed. On the other hand, the micro-
structure of the specimen sintered at $0.67T_m$ was somewhat
complicated consisting of small grains and contained a
small amount of closed pores as shown in Fig. II-5 (e),
which was quite different from the others shown in Fig.
II-5. It is considered that the change of microstructure
at $0.67T_m$ is due to the plastic deformation of particles
which occurred at the ductile temperature range of Si.

In Fig. II-6, the temperature dependence of micro-
structure of Si bodies prepared by the sintering of 0.056
μm particle size powders at 1.0 GPa for 1 minute under
various temperatures are shown. The relative density of
each specimen was already presented in Fig. II-3. The
grain morphologies shown in (b), (c) and (d) were entire-
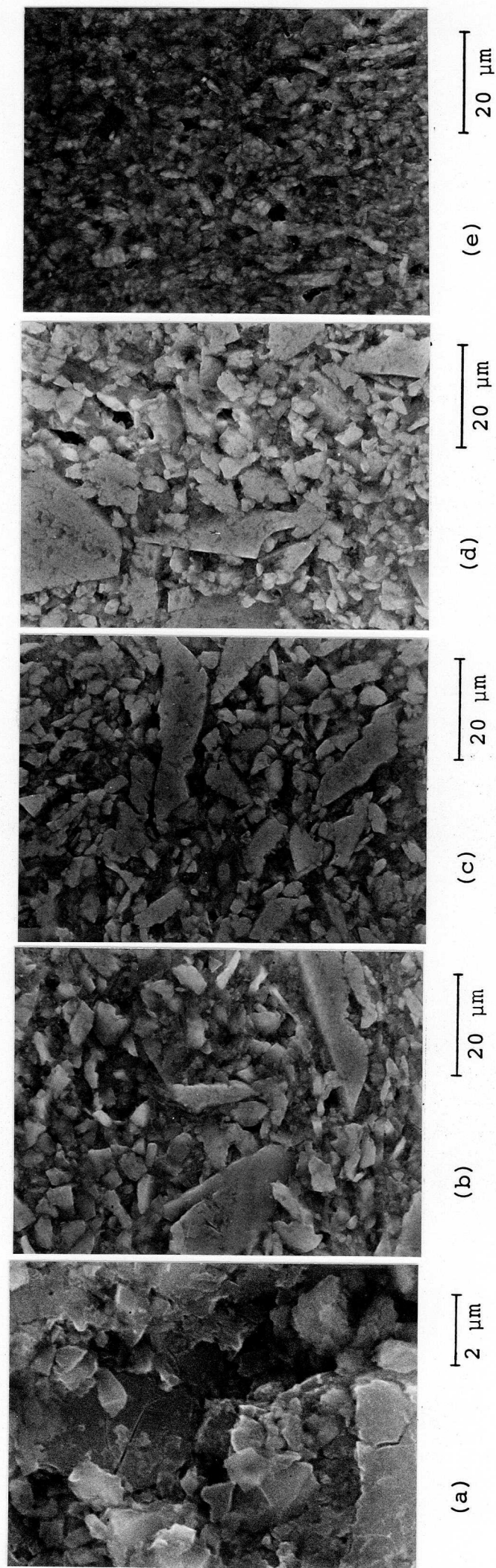ly the same as that of (a) for the green compact com-

Fig. II-5 Microstructures of silicon bodies sintered at (a) $0.19T_m$ (R.T.), (b) $0.40T_m$, (c) $0.51T_m$, (d) $0.59T_m$ and (e) $0.67T_m$ for 4 minutes under 3.0 GPa using the starting powder with the grain size of 0.88 μm.
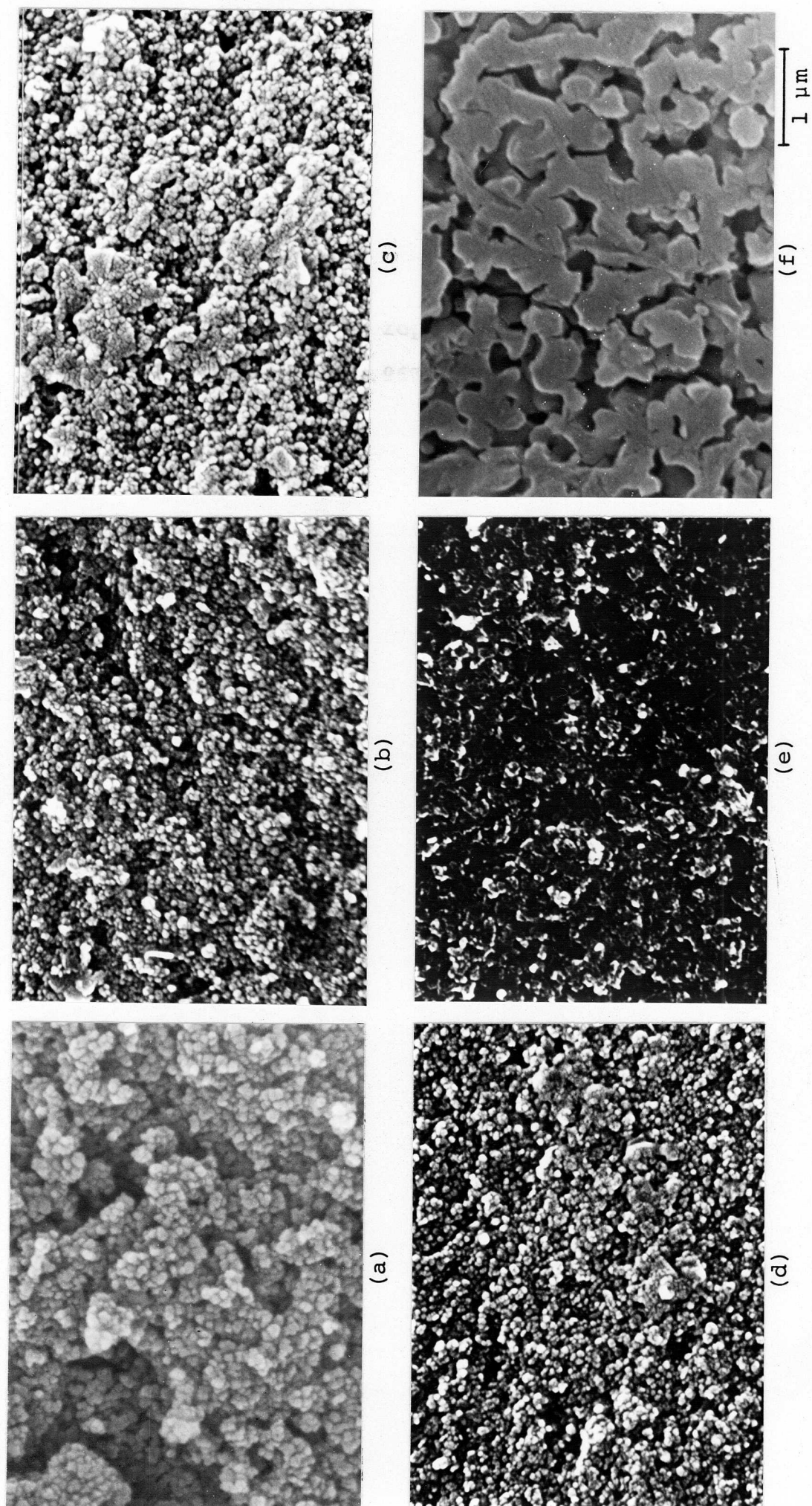
Fig. II-6 Microstructures of silicon bodies sintered at (a) $0.18T_m$ (R.T.), (b) $0.40T_m$, (c) $0.50T_m$, (d) $0.60T_m$, (e) $0.70T_m$ and (f) $0.80T_m$ for 1 minute under 1.0 GPa using the starting powder with the grain size of 0.056 μm.

pressed at room temperature. Plastic deformation was obviously observed in (e) and (f). Especially, the etched surface (f) of the high pressure sintered specimen at $0.80T_m$ showed the well self-bonded microstructure constructed with fine grains, and was quite similar in grain morphology with that reported by Greskovich and Rosolowski, which was fired at $0.96T_m$ for 1 hour in argon atmosphere using 0.23 μm Si powders as starting material.

Fig. II-7 shows the sintering time dependence of microstructure of Si bodies sintered at $0.50T_m$ and 1.0 GPa using 0.056 μm particle size powders as starting material. There seems to be no difference among these three structures. Therefore, it is considered that the morphology of the high pressure sintered Si body did not change during the sintering time of 120 minutes at the brittle temperature range due to the small diffusion coefficient of Si.

Representative fracture surfaces of HIP treated Si at 10 MPa and 100 MPa are presented in Fig. II-8. The starting powder consisting of 0.056 μm particles was cold pressed at 100 MPa. It is evident from these photographs that the grain growth was remarkably prevented by application of high pressure and the diameter of closed pores for the specimen sintered at 100 MPa is much smaller than those at 10 MPa.

II-3   High Pressure Sintering of Titanium Carbide

In the high pressure sintering of TiC, two kinds of powders were used as starting material. The average
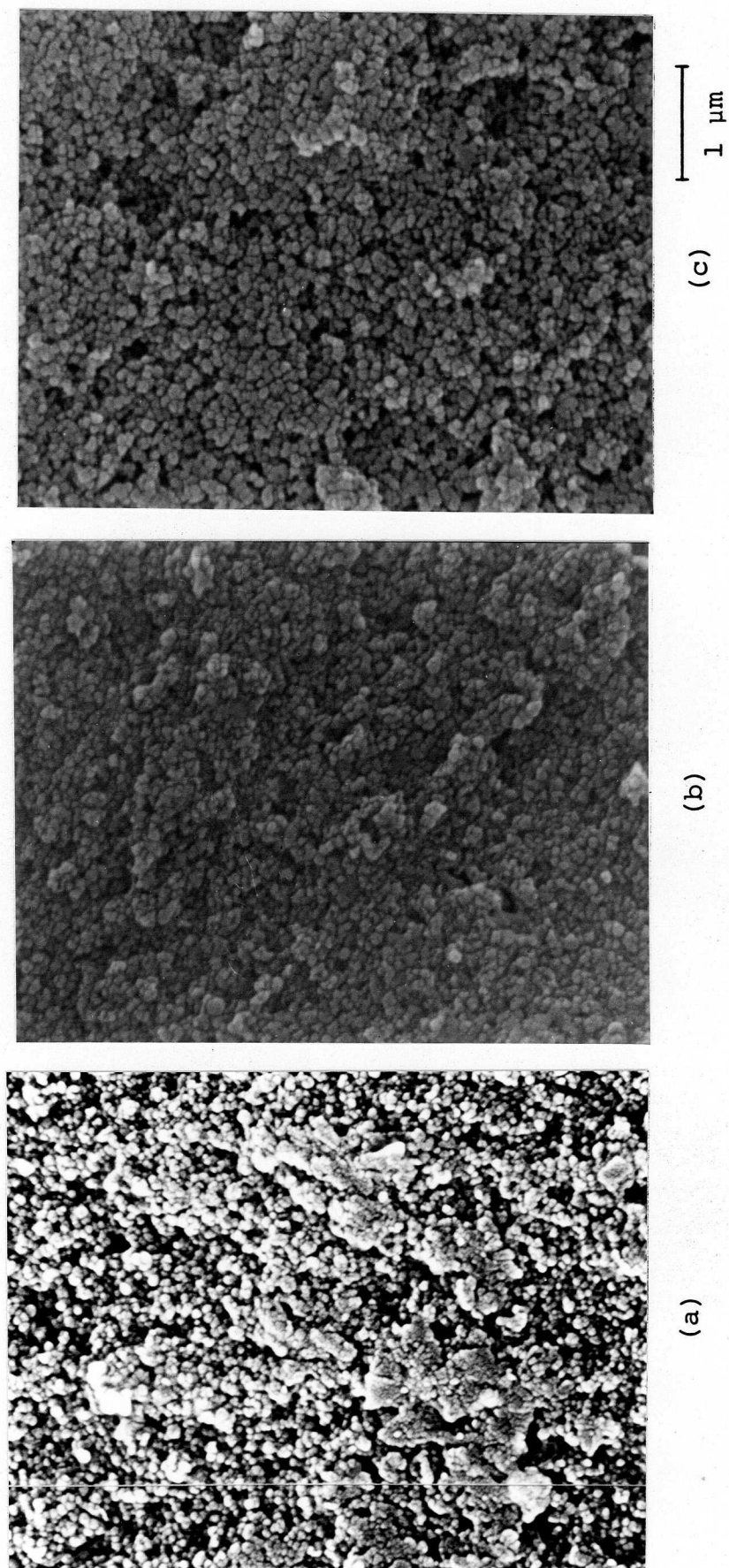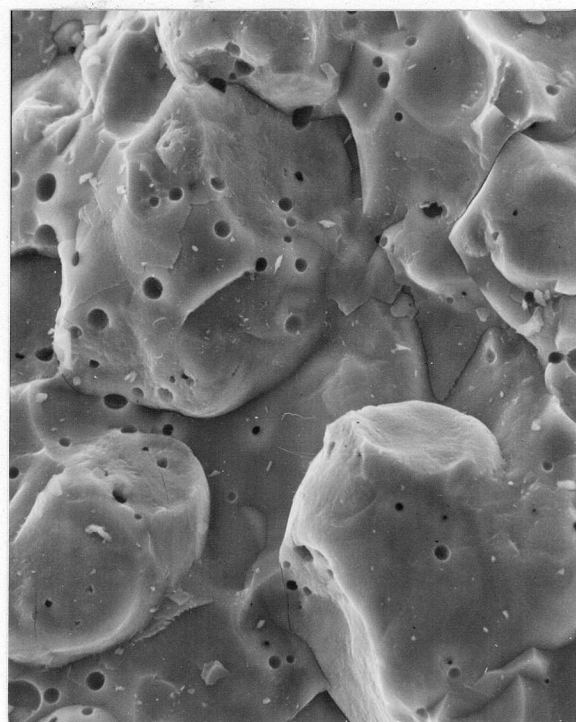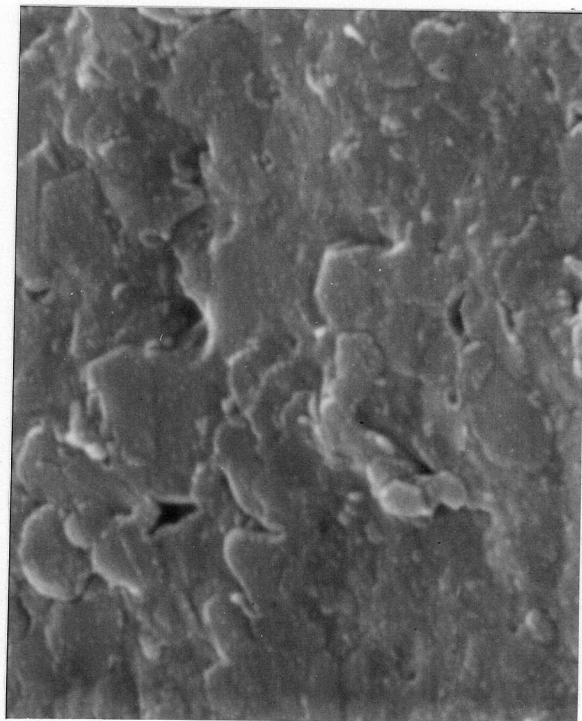
Fig. II-7 Microstructures of silicon bodies sintered at $0.50T_m$ for (a) 1 min, (b) 60 min and (c) 120 min under 1.0 GPa using the starting powder with the grain size of 0.056 μm.

Fig. II-8 Fracture surfaces of silicon bodies fabricated by HIP at $0.80T_m$ for 60 minutes under (a) 10 MPa and (b) 100 MPa using the starting powder consisting of 0.056 μm particles.

particle sizes were estimated to be 1.3 μm* (purity 99.7

%) and 0.07 μm** (99.5%) from the results of specific sur-

face area measurement with BET method. Fig. II-9 shows

the results of the high pressure sintering at various

conditions. At every run, the sintering duration was

kept for 30 minutes. In case when coarse powder was used

as the starting material, the relative density gradually

increased with increasing the temperature, but the relative

density of the sintered bodies obtained from fine powder

reached a constant value of 92 % above 1000°C. This con-

stant value seems to be an end-point density. This be-

havior of the fine powder is thought as follows. At the

temperature range below 1000°C, the toughness of TiC fine

particle is large enough to prevent the fragmentation

induced by the effective stress of the applied pressure.

Besides, consolidation by the particle rearrangement is

also hindered due to the large friction between particles.

At the higher temperature conditions, although both

surface and grain boundary diffusions become remarkably

dominant to promote the densification rate, they hardly

contribute to the densification in case of fine powder.

The temperature dependence of the relative density of

TiC was shown in Fig. II-4 (a), and also the temperature

dependence of the Vickers microhardness reported by

Kohlstedt[50] was shown in Fig. II-4 (b). As seen in both

---

* Kennametal Inc.
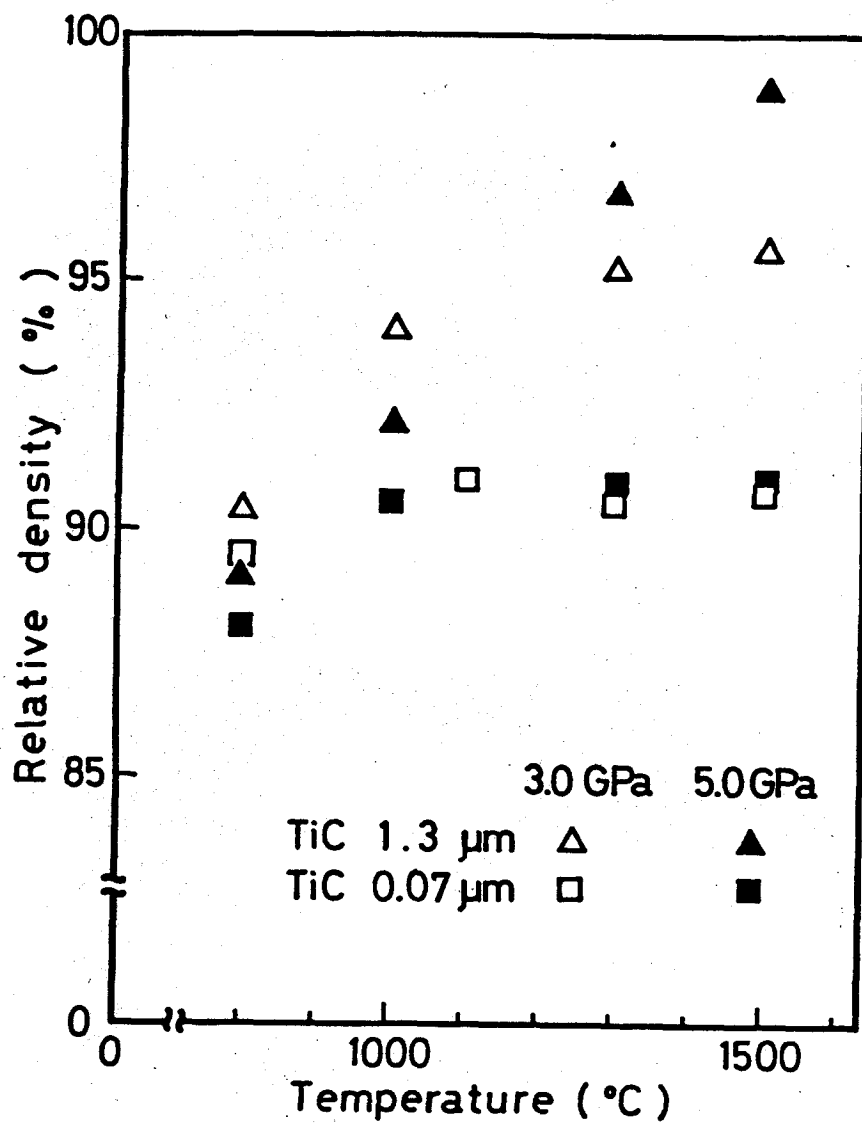
** Toho Titanium Co. Ltd., Japan

Fig. II-9 Relative density versus temperature at constant pressure and run duration for two kinds of TiC powders.

figures, it is expected that the rapid densification due to the plastic deformation is induced by the brittle-ductile transition of TiC at $0.2 - 0.3T_m$.

The temperature dependence of microstructure of TiC high pressure sintered in isobaric conditions using the startin powder consisting of 0.07 μm particles is shown in Fig. II-10. The relative density of the specimens whose surfaces are presented in this figure was already shown in Fig. II-4 (a). It is seen in Fig. II-10 that the morphological change is observed at temperatures above $0.30T_m$ and formation of polyhedron and remarkable grain growth are observed on thespecimens sintered at this temperature range. Comparing microstructure of TiC shwon in Fig. II-10 with that of TiC in Fig. II-6, it is noted that there is a quite difference in grain morpholo-gy between TiC and Si. In case of TiC, although the formation of polyhedron is remarkable, the well developed self-bonding of particles is not observed but inter-granular fracture surfaces are seen as shown in Fig. II-10 (d), (e) and (f).

Fig. II-11 shows the sintering time dependence of microstructure of high pressure sintered TiC in isother-mal conditions using the starting powder consisted of 1.3 μm particles. These specimens had the same relative density of 94 - 95 % of the theoretical density. Taking the mechanical property of sintered ceramics into account, although highly dense bodies can be obtained in a short run in case of the high pressure sintering, it is required to proceed a long run of the high pressure sintering in
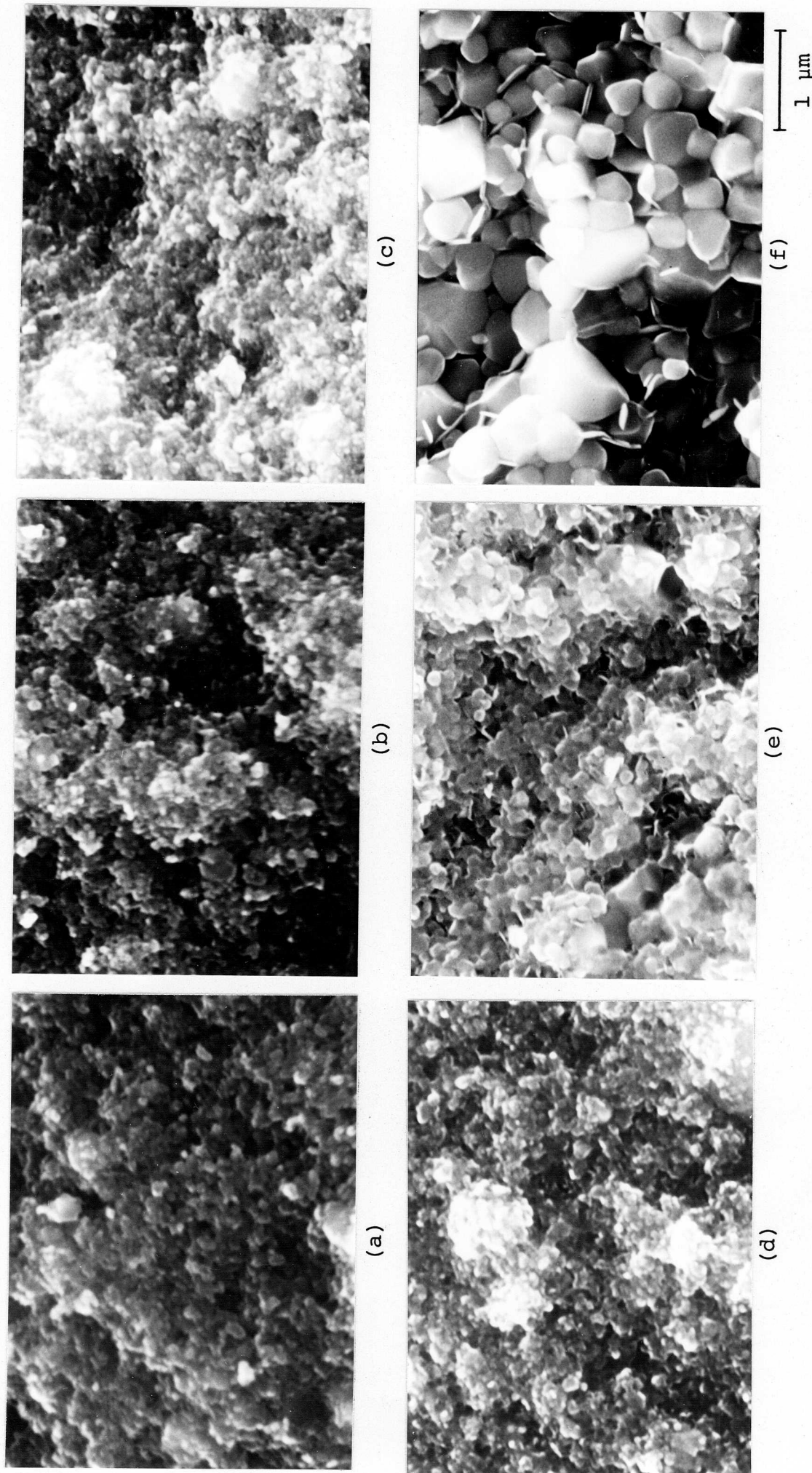
Fig. II-10 Microstructures of TiC bodies sintered at (a) 0.08T_m (R.T.), (b) 0.20T_m, (c) 0.25T_m, (d) 0.30T_m, (e) 0.35T_m and (f) 0.40T_m under 1.0 GPa for 10 minutes using the starting powder consisted of 0.07 μm particles.
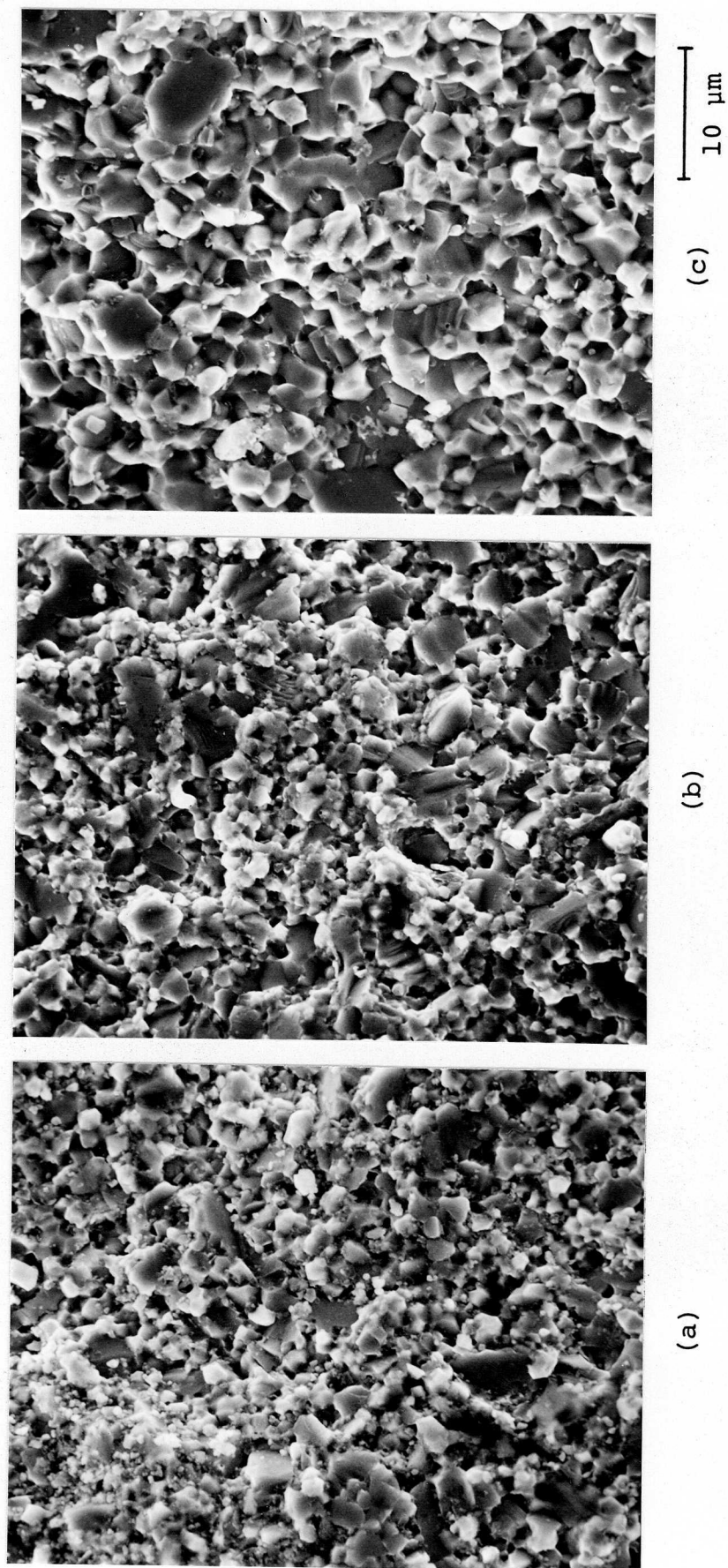
Fig. II-11 Microstructures of TiC bodies sintered at $0.50T_m$ and 3.0 GPa for (a) 5 min, (b) 30 min and (c) 120 min using the starting powder consisted of 1.3 μm particles.

order to obtain strongly self-bonded ceramics.

II - 4   Densification Mechanism in High Pressure Sintering

The present results of the densification behaviors of Si and TiC indicate that there is no agreement between the densification curve obtained from the present experiments and those given to the various sintering models proposed by several other investigators.[7-11] It may be due to the fact that the densification rate in the present study of pressure sintering is too large to apply the sintering models proposed for normal sintering. Therefore, the author has tried to deduce the densification mechanism the observing the change of mechanical property and microstructure during an early stage of high pressure sintering. This attempt led a conclusion that fragmentation and rearrangement of particles could be an operative mechanism in the brittle region in the initial stage of pressure application, and that, on heating, the particle rearrangement and plastic flow became dominant to promote the densification rate.

The proposal model is shown in Fig. II-12. At relatively low temperatures where the materials have brittle characters, the densification of the specimen occurs due to the fragmentation and rearrangement of the particles. · In this temperature region, therefore, the pressure dependence of densification is remarkable. At higher temperature region where the materials have the ductile characters, the densification takes place abruptly accompanied by the plastic deformation mechanism due to the brittle-ductile transition.

Densification Mechanism under High Pressure

Brittle region   **Ductile region**

Fragmentation

$\xrightarrow{\hspace{1.5cm}}$ Plastic deformation

Rearrangement   **(T)**

Fig. II-12 Schematic diagram showing densification mechanism under high pressure.

Closed pores are formed in case when the magnitude of effective stress of applied pressure is smaller than that of toughness of the material, and consequently further densification is not proceeded.

Chapter III

Diffusion Phenomena under Quasihydrostatic
High Pressure

III - 1   Introduction

The volume diffusion under high pressure is discussed
in this chapter. In case of pressure-less sintering, the
driving force for densification is induced by the differ-
ence between surface energy and grain boundary energy.
During the initial stage of sintering, matter can move
through the paths for mass transport of particle surface,
particle bulk and/or grain boundary between particles
according to surface, lattice and/or grain boundary dif-
fusions.[51]   Each path has a proper role in mass trans-
port. Among them, only a transfer of matter from the
particle volume and/or from the grain boundary between
particles due to lattice diffusion causes shrinkage and
pore elimination.

In pressure sintering, even if a rapid densification
occurrs according to fragmentation, rearrangement and
plastic deformation in the initial stage of sintering,
the densification at the final stage and the self-bondings
of particles strongly are affected on the mass transpor-
tation under pressures, that is, the diffusion of con-
stituent elements.

It is generally knwon that the densification is
performed in a shorter sintering time in case of pressure

sintering. Since Herring [52] proposed the model of diffusion creep mechanism under pressure, various modifications have been made, [53,54] and it is understood that a rapid densification at the final stage of pressure sintering is promoted by the stress enhanced diffusion due to the inhomogenity of the stress in a particle.

On the other hand, it is well known in thermodynamical treatment that the diffusion coefficient decreases under hydrostatic pressure, especially for the vacancy mechanism difuusion. In fact, Hudson and Hoffman [55] investigated the effect of hydrostatic pressure on the self-diffusion in lead, and obtained result that the apparent self-diffusion coefficients in lead decreased an order of magnitude by the application of hydrostatic pressure of 1.0 GPa. There are several studies on the effect of pressure on coefficient of diffusions such as self-diffusion in metals and mutual-diffusion in alloys. However, no studies has been conducted so far on the mutual diffusion under pressure in intermetallic compounds such as TiC.

A volume diffusion dominantly controls a densification rate at the final stage of pressure sintering and the self-bonding of particles. From this view-point, an investigation on the diffusion phenomena in intermetallic compounds under pressure is important for the promotion of the self-bonding of particles, which is strongly related to the mechanical strength of the sintered body.

III - 2   Experimental

A diffusion coefficient is usually determined by one of the following three methods; 1) EPMA method, 2) tracer method and 3) layer growth method.

In this study, the layer growth method was adopted. In this case, the following assumptions are made.

1. The diffusion coefficient in each phase is independent of concentration.

2. Phase boundary equilibria are virtually established.

3. The solubility of transition metal in graphite is negligible, hence diffusion of metal into graphite can be neglected.

4. Diffusion in metal phase is so rapid in comparison with that in carbide that the latter diffusion is only considered as rate-detrmining.

5. The specific volumes of carbide and metal phases are essentially equal, so that the graphite-carbide interface is fixed with reference to the marker.

In Ti-C system, the self-diffusion coefficient of Ti (D_m) is smaller in some orders of magnitude than that of graphite (D_c). And the product ($V_c \cdot C_c$) of molar volume (V_c) and the concentration of graphite (C_c) is less than a tenth of that of Ti ($V_m \cdot C_m$). The mutual diffusion coefficient is, therefore, reduced to;

$$\widetilde{D} = D_m V_c C_c + D_c V_m C_m \fallingdotseq D_c V_m C_m$$

Wagner[56] examined the present type of diffusional phase formation and reported that the diffusivity of carbon in carbide was related to the parabolic rate constant (K) by the following equations, provided that the diffusivity was independent of the carbon concentration.

- 45 -

$$\frac{C_s - C_m}{C_m - C_o} = \pi \exp(\gamma^2) \operatorname{erf}(\gamma)$$

$$4\gamma^2 D = K$$

where γ is a dimensionless constant. Carbon concentration C_s, C_m and C_o are designated in Fig. III-1 and whose values are obtianed from the phase diagram of Ti - C system (Fig. III-2). The parabolic rate constant is referred to the thickness of the carbide layer (τ) and annealing time (t);

$$\tau^2 = K t$$

Combining the equations mentioned above, the diffusion coefficient is given as follows;

$$D = \frac{1}{4\gamma^2} \frac{\tau^2}{t}$$

In order to simplify the analysis of the kinetics of layer growth, two assumptions are added.

6. The carbon concentration across the carbide layer varies linearly.

7. The amount of carbon given to the carbide layer from the carbon-saturated metal is negligible.

The solution accordingly is

$$D = \frac{1}{4}\left(\frac{C_s + C_m}{C_s - C_o}\right) \frac{\tau^2}{t}$$

In the present high pressure experiments, the cubic anvil type high pressure apparatus was used. The diffusion couples of Ti disks and graphite disks with platinum markers were prepared. The Ti disks ($5^\phi \times 2^t$ mm) were cut
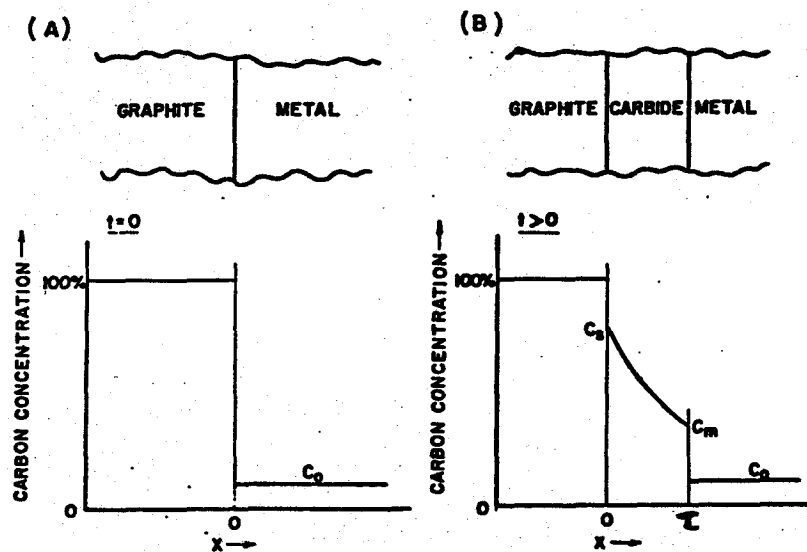
Fig. III-1 Concentration profile at graphite-
metal interface; (A) initially, (B) after the
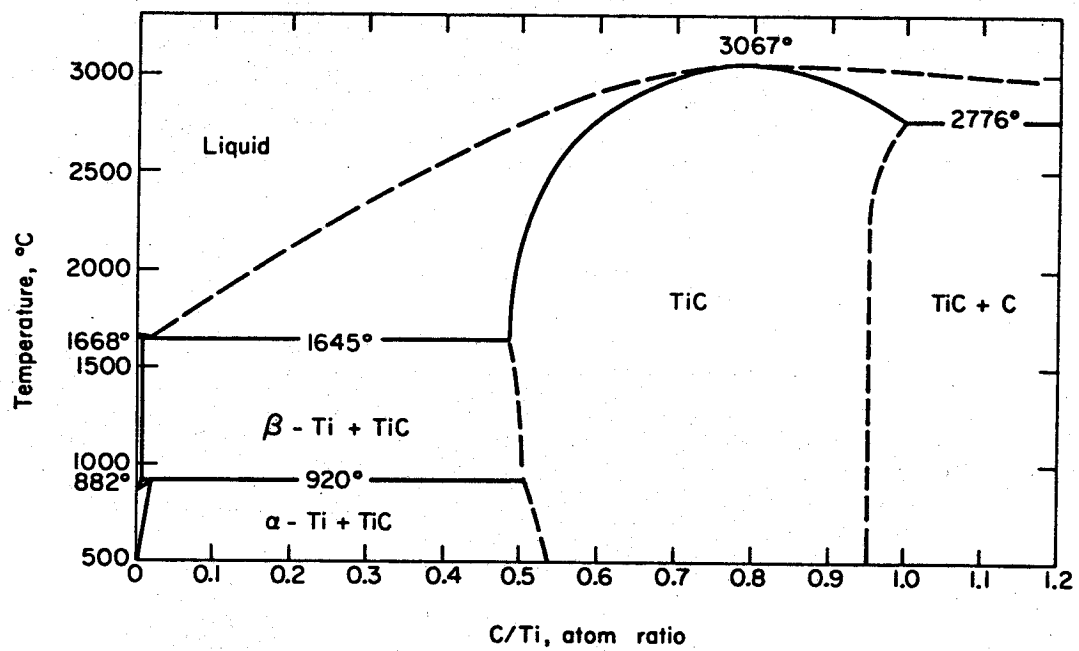formation of a carbide layer. (from Vansant
et al.[57])

Fig. III-2 Phase diagram of Ti – TiC system.
(from McCreight[58])

off from the commercial pure titanium bar[*] and annealed
at 1050°C for 4 hours, in order to prevent the grain
boundary diffusion. The graphite disks (5^ϕ x 1^t mm) were
cut off from the commercial graphite bar.[**] Using these
diffusion couples of Ti and C, the high pressure experi-
ments were conducted under various conditions as follows.

Temperature : 1200, 1300, 1400, 1500°C

Pressure   : 1.0, 3.0 GPa

Duration   : 30 - 810 min

III - 3 Diffusion Coefficients under Quasihydrostatic
         High Pressure

SEM micrographs of the cross sections of diffusion
annealed specimens are illustrated in Fig. III-3. The
specimens were cut parallel to the diffusion flow of
carbon using a diamond cutter and etched with the mixture
of fluoric acid and nitric acid after smoothing the sur-
faces. By measuring the thickness of TiC layers, layer
growth constants and diffusion coefficients were calcu-
lated.

Arrhenius plots of the diffusion coefficients under
1.0 and 3.0 GPa are shown in Fig. III-4. There seems to
be no notable difference in diffusion coefficients between
1.0 and 3.0 GPa. Vansant and Phelps[57] measured the
temperature dependence of the diffusivity of carbon in
TiC using the planar diffusion couples of Ti and graphite
disks under pressure-less condition. Their results are

---

*   Japan Lamp Industrial Co. Ltd., Japan

**   Tokai Denkyoku Co. Ltd. Japan, G-2080

graphite

TiC

Ti

1400°C

1200°C

120 min

120 min

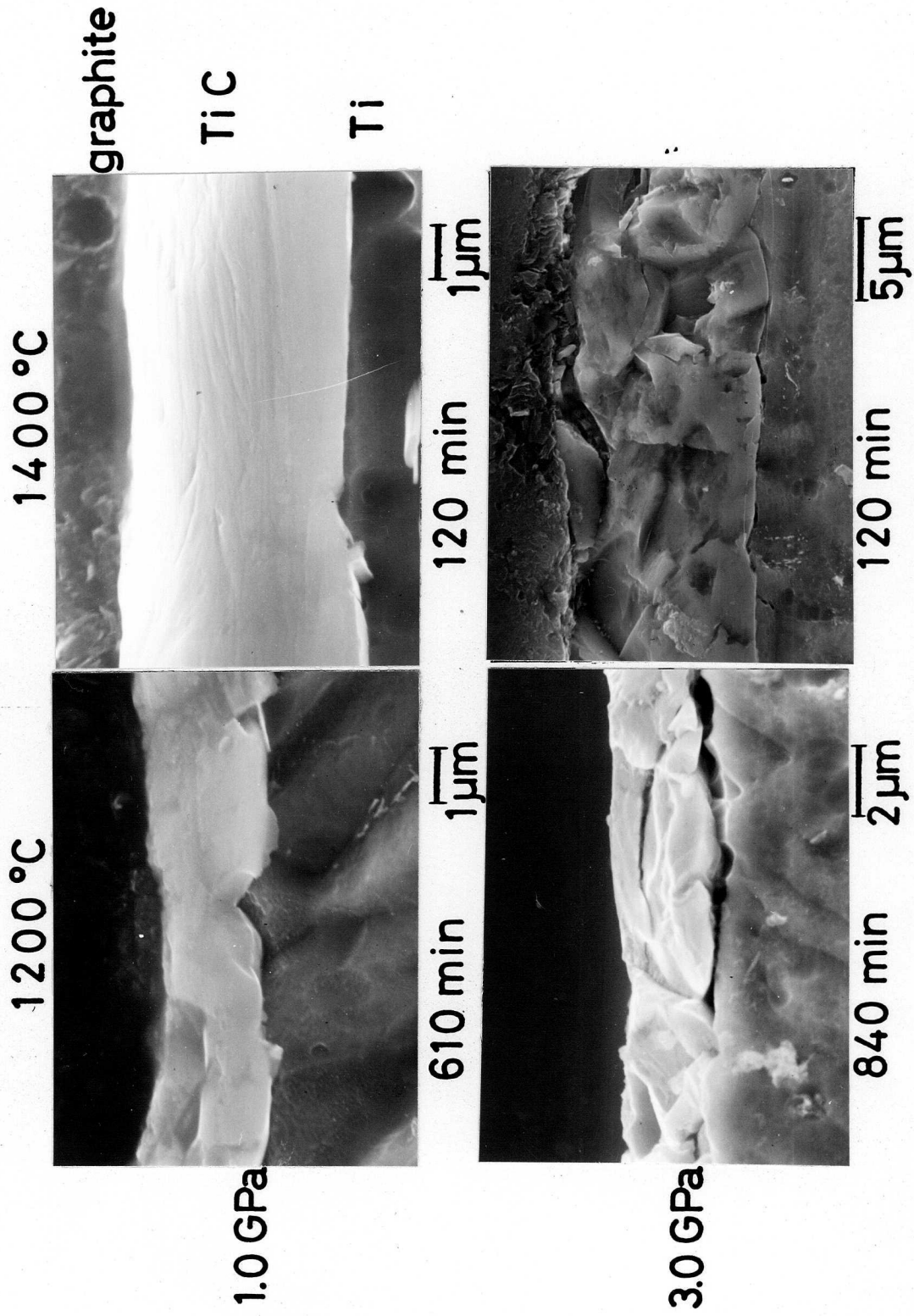610 min

840 min

1.0 GPa

3.0 GPa

Fig. III-3　SEM photographs of cross sections of diffusion couples

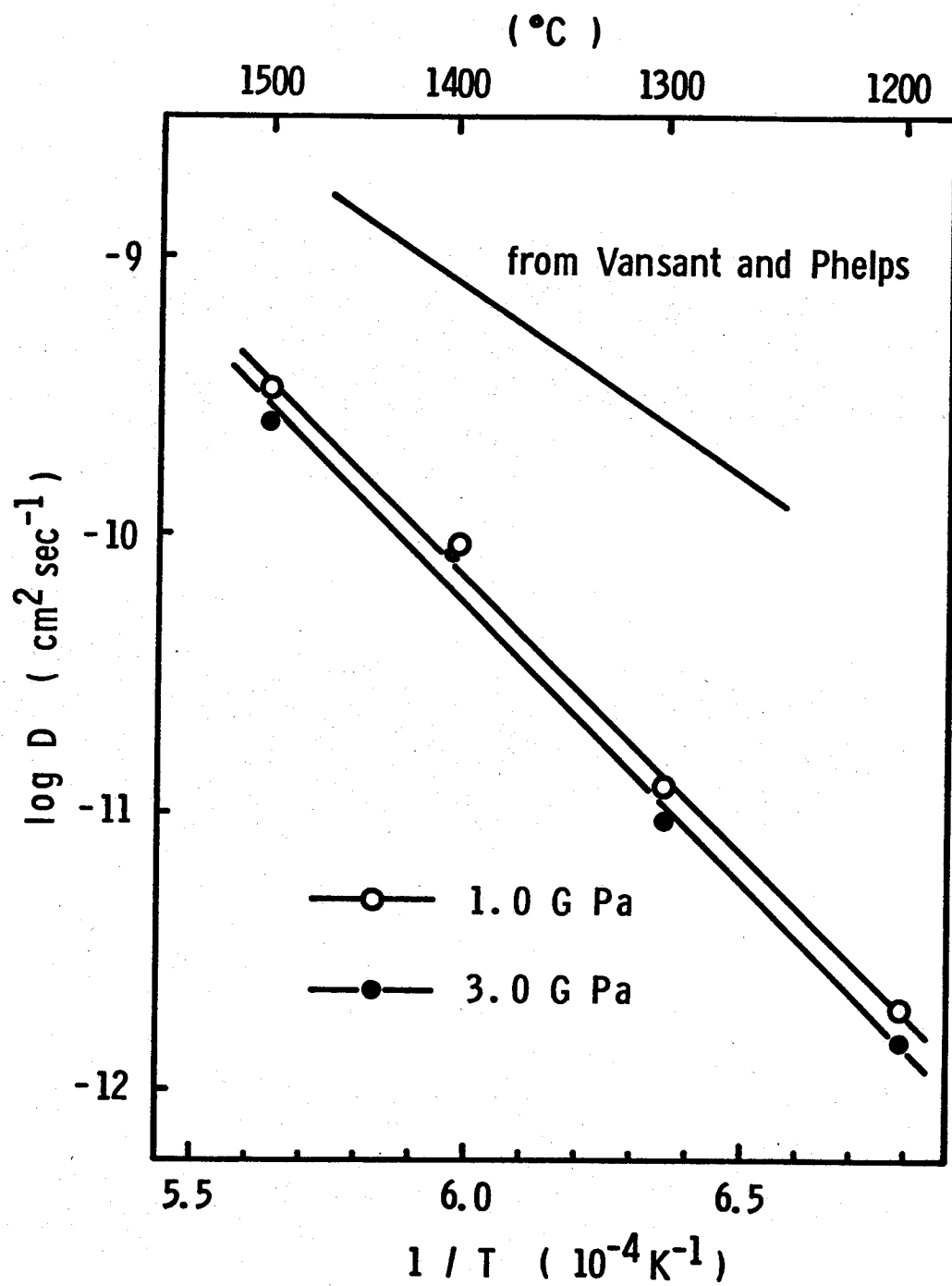annealed at 1200°C and 1400°C under 1.0 and 3.0 GPa.

Fig. III-4   Temperature dependence of diffusivity
of carbon in TiC.

also shown in Fig. III-4. Comparing the results of the present work with that by Vansant and Phelps in the temperature range from 1200°C to 1500°C, it is evident that the diffusion coefficients of carbon in TiC are by an order of magnitude smaller under quasihydrostatic high pressure conditions than under pressure-less conditions.

The temperature dependences of teh diffusion coefficients are as follows.

1.0 GPa $D = (4.01 \times 10) \exp(-\frac{(3.75 \pm 0.18) \times 10^5}{RT})$

3.0 GPa $D = (5.48 \times 10) \exp(-\frac{(3.83 \pm 0.25) \times 10^5}{RT})$

$$(cm^2 sec^{-1})$$

(from Vansant and Phelps)

Pressure-less $D = (1 \times 10^{-1}) \exp(-\frac{(2.59 \pm 0.38) \times 10^5}{RT})$

There are no remarkable difference in the activation energies of diffusion under 1.0 and 3.0 GPa, but these values are much larger than that of pressue-less condition.

There results are understood by the following concept; when the crystalline lattice is homogeneously compressed under the quasihydrostatic high pressure, the concentration of vacancy decreases and the activation energy for migration of atom increases. The present result indicates that the dominant mechanism of diffusion of carbon in TiC is controlled by vacancy.[58]

III - 4   Sintering Mechanism in High Pressure Sintering

The sintering mechanism of covalent solids was systematically investigated in the present study. The

mechanism are schematically shown in Fig. III-5. The densification mechanism under pressure was already disscussed in the Section 4 of Chapter II. In the first stage of high pressure sintering, the self-bonding of rigid sintered bodies was not proceeded yet and the open pores still existed inside the products. The dominant sintering mechanism after the first stage is the stress enhanced diffusion, because the applied pressure effectively operates as the stress on the contact points of particles. Therefore, the advanced diffusion is induced due to the distortion of the crystalline lattice, and the rapid densification is proceeded.

According to the stress enhanced diffusion, the open pores are eliminated and the closed pores are formed in the sintered body. The retarded diffusion is observed in this stage because of homogeneous distribution of the stress in grains, and concequently the densification of specimen is not obsrved. However, it is important to consider the role of volume diffusion under high pressures to produce the self-bonded sintered ceramics by means of the selection of the most available sintering conditions.

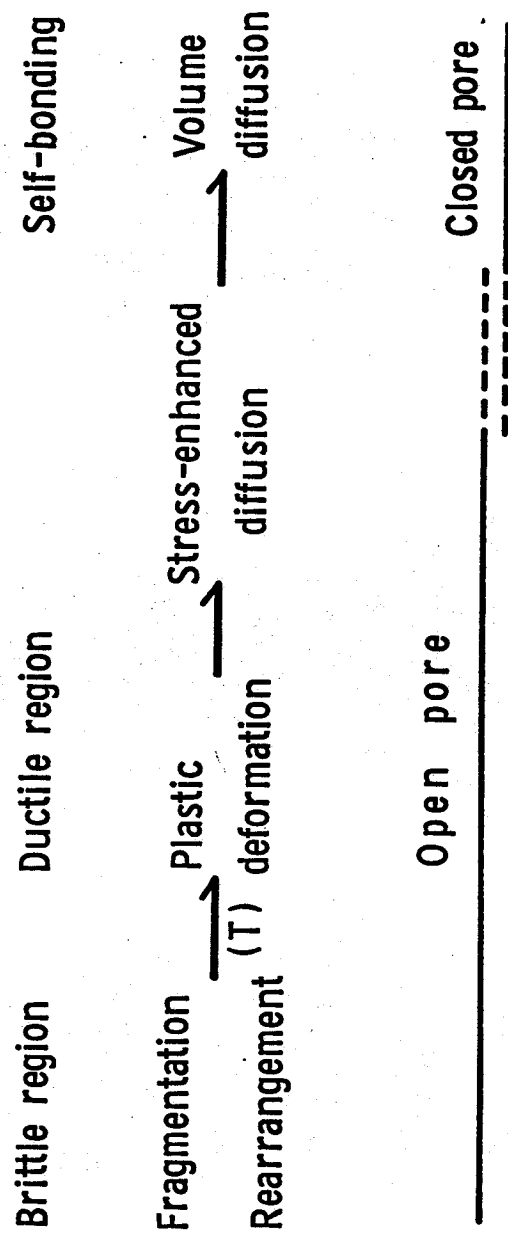# Densification Mechanism and Self-Bonding in High Pressure Sintering

Brittle region   Ductile region   Self-bonding

Fragmentation   Plastic   Stress-enhanced   Volume

Rearrangement   (T) deformation   diffusion   diffusion

Open pore   Closed pore

Fig. III-5   Schematic diagram of densification mechanism and self-bonding in high pressure sintering.

Chapter IV

High Pressure Sintering of Si_3N_4

IV - 1   Introduction

Covalent solids of non-oxide compounds such as silicon nitride (Si_3N_4) and silicon carbide (SiC) are interesting materials in the field of high performance applications.[1-3] These materials are being considered to utilize as the components in gas turbine and internal combustion engine in near future whose operation temperature will be much higher than those used in the present time. The characteristics of these materials are shown in Table IV-1.[59-69] Since it is well known that these covalent solids are difficult to make dense sintered bodies by a normal sintering, it is required very much to fabricate these compounds into dense and strong ceramic bodies with a desired shape by an inexpensive process. For this purpose, a lot of investigations have been proceeded in many laboratories all over the world.

As for sintering of Si_3N_4, it has been found that almost theoretically dense ceramic bodies can be fabricated by the hot-pressing with some amounts of additives such as magnesia (MgO),[13-18] yttria (Y_2O_3)[19-21] and alumina (Al_2O_3).[22,23] The absence of porosity results in ceramic bodies with exceptionally high strengths.[12] However, it is also well known that these additives existed at grain boundaries as the secondary glassy

Table IV-1 Characteristics of Si_3N_4 and $SiC^{59-69})$

	Si_3N_4		SiC	
	α-Si_3N_4	β-Si_3N_4	β-SiC	α-SiC
Crystal structure	hexagonal — a = 7.7608 Å, c = 5.6139 Å	hexagonal — a = 7.6085 Å, c = 2.9111 Å	cubic — a = 4.349 Å	hexagonal — a = 3.07 Å, c = 10.05 Å
Theoretical density (g·cm^{-3})	3.182	3.192	3.21	3.22
Melting point (°C)	$\alpha \longrightarrow \beta$ (1500−1800)	1839*	$\beta \longrightarrow \alpha$ (2000−2300)	2400*
Fabrication method	hot-pressing with Y_2O_3 or MgO	reaction sintering	hot-pressing with B and C	reaction sintering
Porosity (%)**	~ 0	~ 20	~ 0	2 − 3
Thermal conductivity (cal/cm·sec·°C)**	0.134 (R.T.) / 0.051 (1000°C)	0.036 (500°C) / 0.034 (1200°C)	0.15 (500°C) / 0.9 (1200°C)	0.2 (500°C) / 0.1 (1200°C)
Thermal expansion (°C^{-1})**	3.6×10^{-6} (R.T. − 1000°C)	2.5×10^{-6} (R.T. − 1000°C)	4.8×10^{-6}	4.8×10^{-6} (R.T. − 1500°C)
Hardness (GN·m^{-2})**	18 − 20	20	26.3	—
Bending strength** (MN·m^{-2})	1300 (R.T.) / 1000 (1200°C)	290 (R.T.) / 270 (1200°C)	576 (R.T.) / 550 (1400°C)	446 (R.T.) / —

* Decomposition temperature, ** Depend on fabrication conditions

phases, which brought about the drastic fall-down of mechanical strength of sintered bodies at elevated temperatures.[24] There has been continued to study the improvement of the high temperature strength of Si_3N_4 ceramics by approaching the crystallization of glassy phases at grain boundaries.[25] Most of studies, in general, tend to decrease the amount of additives and to find a new additive so as not to occur drastic fall-down of mechanical strength at the temperature range up to 1500°C which is considered as the operation temperature of these ceramics.

An attempt to consolidate Si_3N_4 without additives was performed by Terwillinger and Lange[71] but no densification took place. Prochazka and Rocco[33] investigated the high pressure sintering of Si_3N_4 and resulted that only silicon rich powders could be consolidated to nearly theoretical density under extremely high pressure conditions. It is very important for the high temperature structural materials of Si_3N_4 to improve the new sintering method to fabricate the pure and dense ceramic body and also to make clear the sintering mechanism of Si_3N_4 without any additives under pressure.

Two crystalline phases of Si_3N_4 are known; α- and β- forms.[71] It is generally said that the α-β phase transformation in Si_3N_4 is reconstructive, and that the phase transformation occurrs above 1500°C in the conventional hot-pressing with additives.[72,73] There are few investigations of the effect of the phase transformation on the densification of Si_3N_4 without additives

in the high pressure sintering.[30-35]   In this chapter,

the sintering mechanism of Si_3N_4 under high pressure is

discussed with respect to the effect of the phase trans-

formation on the densification.

IV - 2   Phase Transformation under High Pressure

   Two kinds of powders such as α- and β-Si_3N_4 were

used as starting materials. α-Si_3N_4[*] was 99.9% purity

and its average particle size calculated from the

specific surface area was about 0.25 μm. And α-Si_3N_4

powder used in the present study contained about 4 wt%

β phase. β-Si_3N_4 powder was prepared from α-Si_3N_4 powder

by heat treatment at 1830°C for 3.5 hours under nitrogen

pressure of 8 MPa, and it was ground in a mortar before

use. Free silicon was not detected in either starting

powders or sintered bodies by X-ray powder diffraction

analysis. Using α-Si_3N_4 powder withour additives as

starting material, phase transformation from α- to β-

Si_3N_4 was examined under high pressure-temperatures.

High pressure experiments were carried out under 1.0,

3.0 and 5.0 GPa and at 1600° and 1800°C for various

durations up to 200 minutes. The samples were heated

at the rate of about $50°C \cdot sec^{-1}$, and after maintaining

at the desired temperature, they were quenched to room

temperature.

   Figs. IV-1, 2 and 3 show the time dependences of

the β phase weight fractions of sintered specimens. In

these figures, flash indicates the subsequent quenching

_____

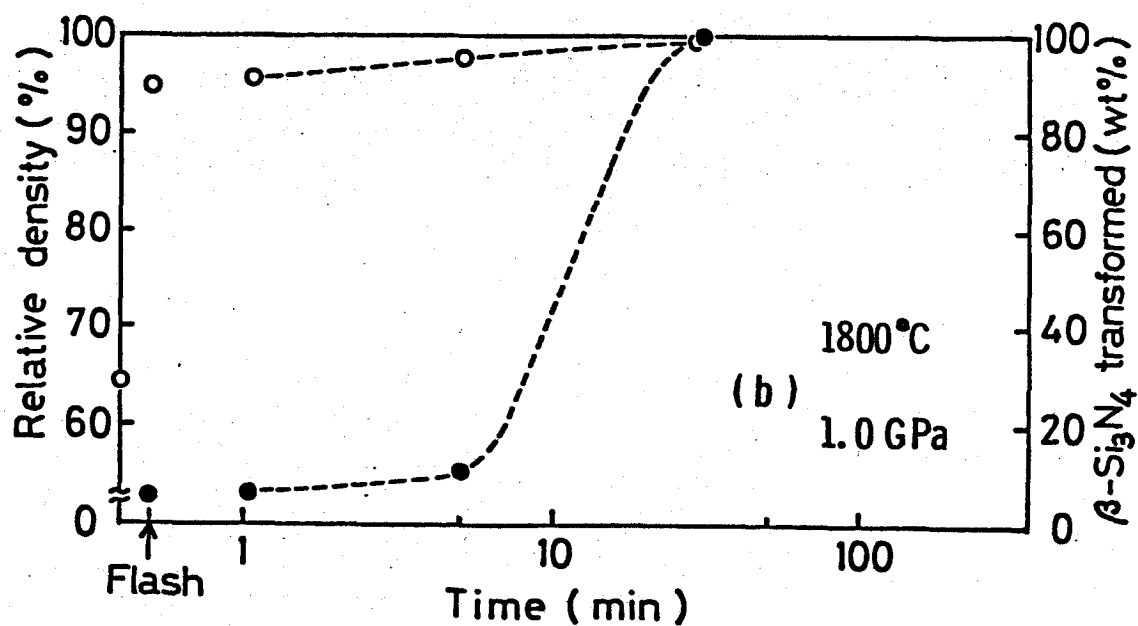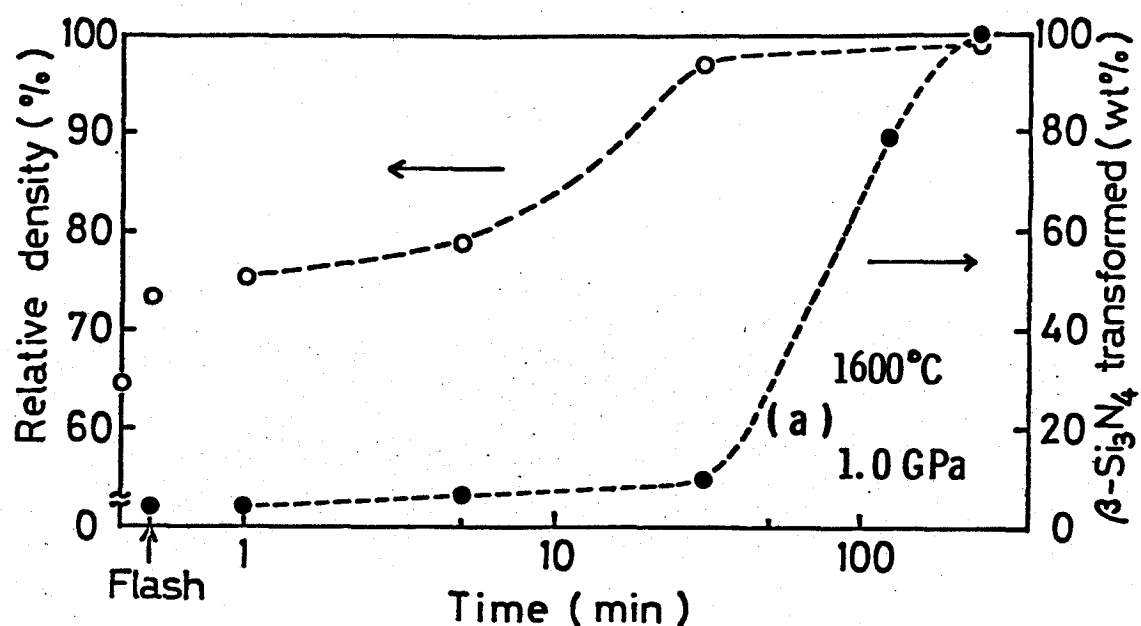[*] H. C. Starck, Berlin, H - 1 class

Fig. IV-1　Time dependence of densification and of phase transformation of pure Si_3N_4 sintered at (a) 1600°C and (b) 1800°C under the constant applied pressure of 1.0 GPa.
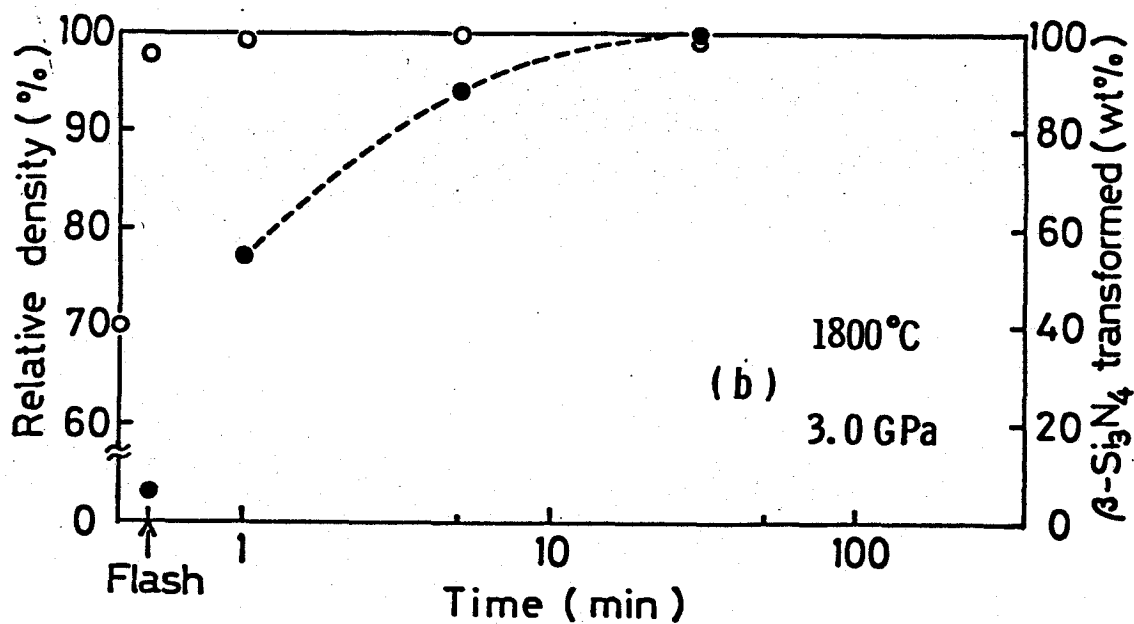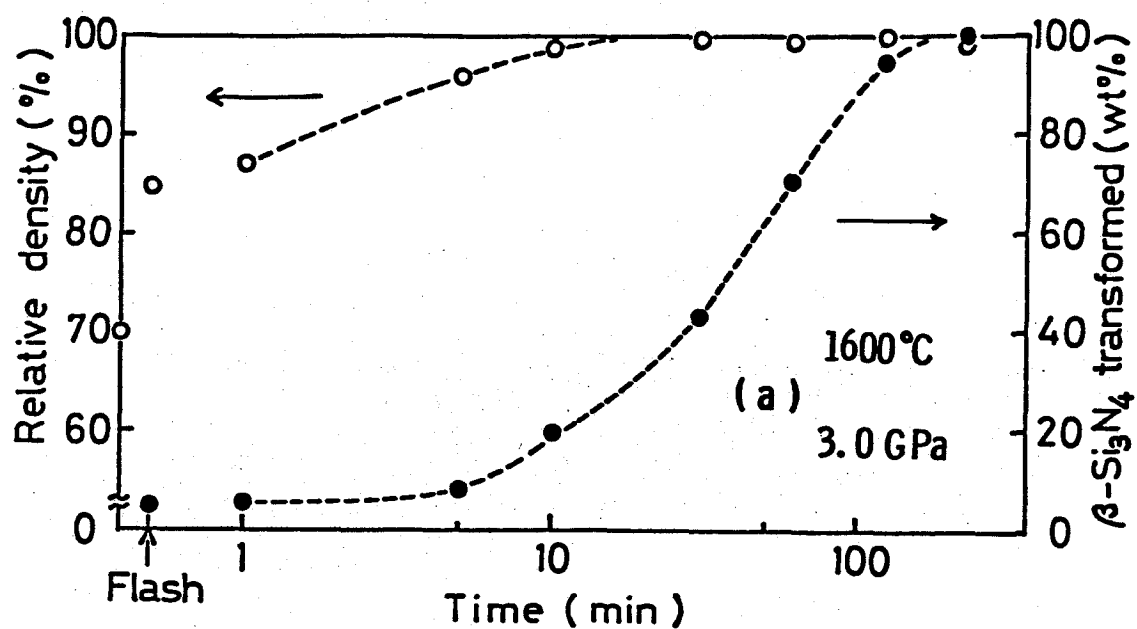
Fig. IV-2 Time dependence of densification and of phase
transformation of pure Si_3N_4 sintered at (a) 1600°C and (b)
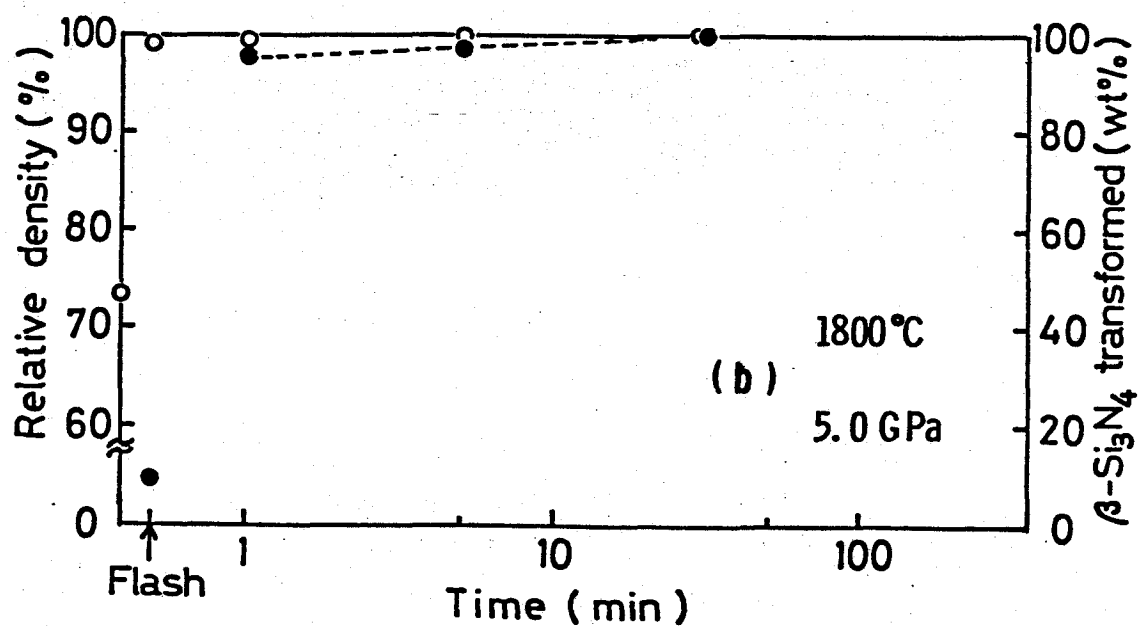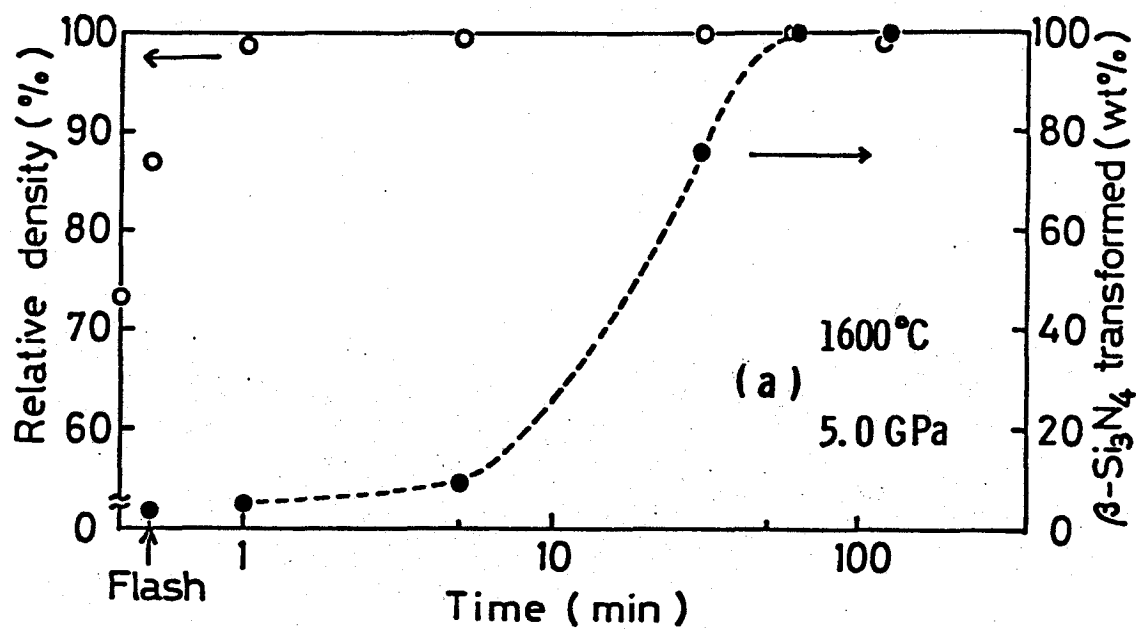1800°C under the constant applied pressure of 3.0 GPa.

Fig. IV-3 Time dependence of densification and of phase transformation of pure Si_3N_4 sintered at (a) 1600°C and (b) 1800°C under the constant applied pressure of 5.0 GPa.

after heating up to the desired temperatures. The phase transformation did not occur by flash treatment. Remarkable phase change did not proceed in a short sintering time up to 5 minutes at 1600°C and 1800°C under 1.0 GPa, 1600°C under 3.0 and 5.0 GPa, respectively. At 1800°C, on the other hand, a rapid phase transformation occurred within 1 minute under 3.0 and 5.0 GPa. The weight fraction of β phase gradually increased with increasing the sintering time under any pressure-temperature conditions except for the condition of 1800°C at 5.0 GPa, and the specimen consisting of single phase β-Si_3N_4 was obtained even at the condition of 1600°C under 1.0 GPa by long sintering duration of 200 minutes. As seen in Figs. IV-1, 2 and 3, the phase transformation from α- to β-Si_3N_4 was accelerated by heating at high temperatures and the application of higher pressure.

The densification behaviors of α-Si_3N_4 are also shown in Figs. IV-1, 2 and 3. Dissimilarly to the results of phase transformation, remarkable changes in the relative densities of sintered bodies are observed by the flash treatment. As seen in these figures, sintering time dependence exists in densification behavior of α-Si_3N_4. Although the densification rates without additives under the present investigation were much slower than those hot-pressed with 5 wt% MgO at 20 MPa,[72] almost theoretically dense specimen of Si_3N_4 was obtained without additives under the condition at 1600°C and 1.0 GPa for a long sintering duration as seen in Fig. IV-1. The time dependence of densification

of α-Si_3N_4 is quite different in manner from the results of Si and TiC in Chapter II. This result attributes to the contribution of the phase change of Si_3N_4 or the stress enhanced diffusion. To make clear the densification mechanism of Si_3N_4, the role of the phase transformation on densification behavior of Si_3N_4 was investigated.

The effect of the difference of starting powders on densification is shown in Fig. IV-4. As seen in this figure, there seems that no difference exists in the densification behavior between α-Si_3N_4 and β-Si_3N_4 as starting material. This result indicates that the densification of pure Si_3N_4 does not depend on the difference of phases in the starting powders.

The microstructures of the specimens were observed by SEM. The time dependence of fracture surfaces of the high pressure sintered specimens for α-Si_3N_4 is shown in Fig. IV-5. From these photographs and the results of the phase transformation and the densification as shown in Fig. IV-2 (a), it is considered that morphology of Si_3N_4 obviously changed with the progress of densification and phase transformation during high pressure sintering without additives. The fracture surface of the specimen sintered for 10 minutes revealed the beginning of the formation of polyhedrons. The specimen sintered for 60 minutes showed the surface having transgranular fractures of well self-bonded polyhedrons whose average particle size was about 1 μm.
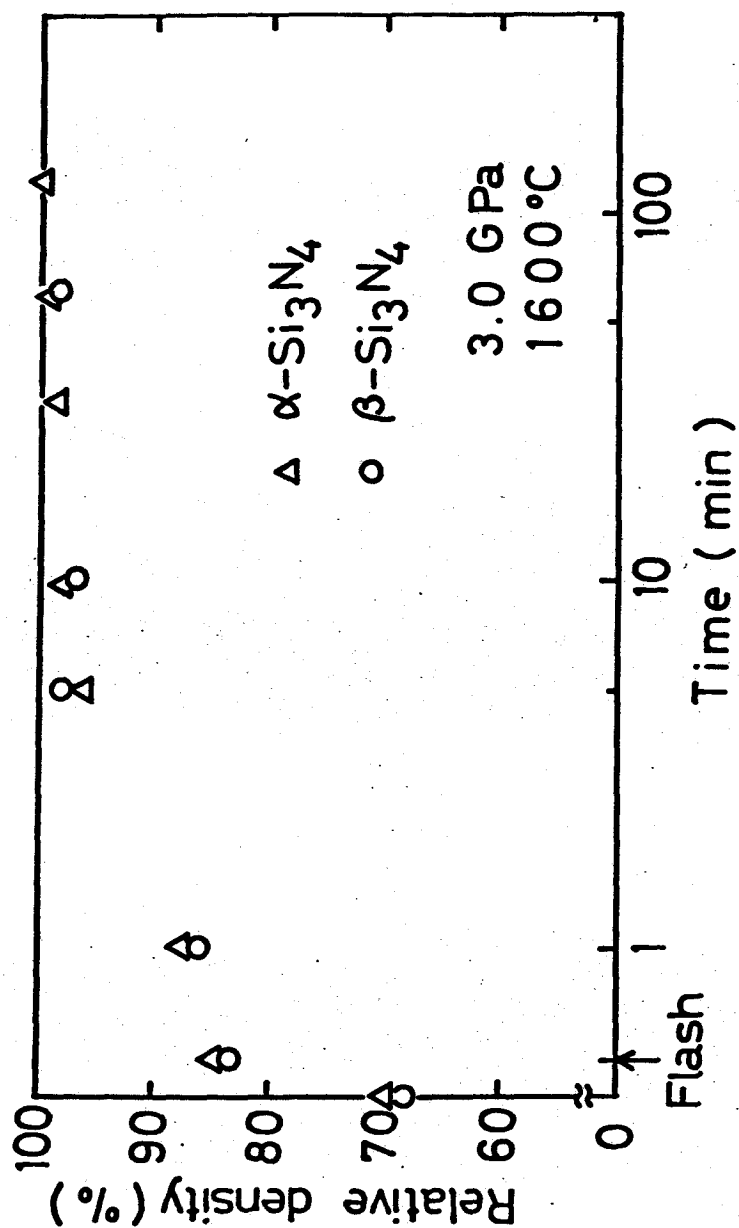
Fracture surfaces of high pressure sintered specimens

- 63 -

Fig. IV-4 Time dependences of relative density of Si_3N_4 bodies
sintered from two kinds of starting powders without additives
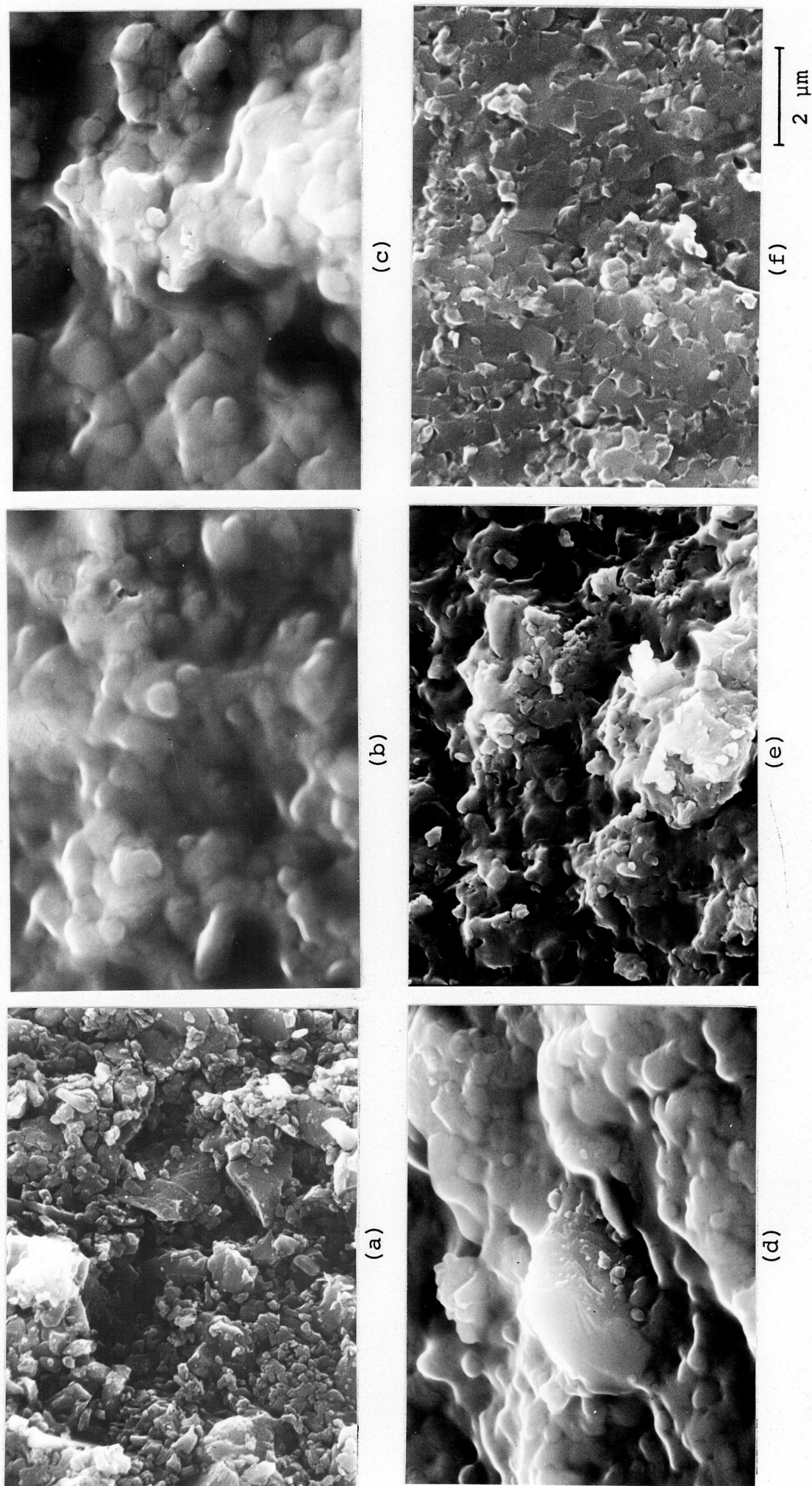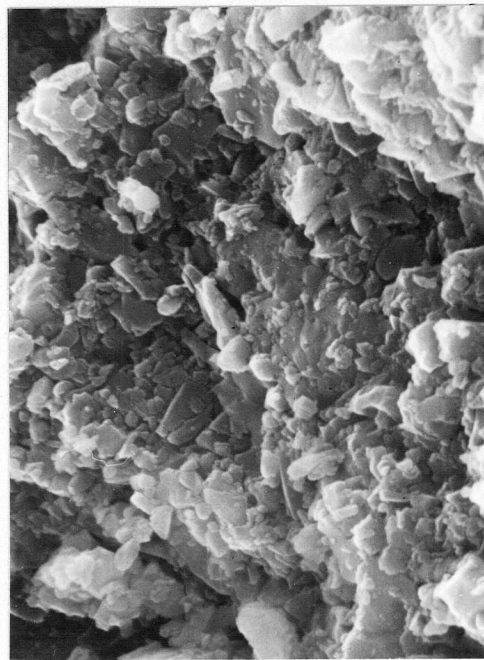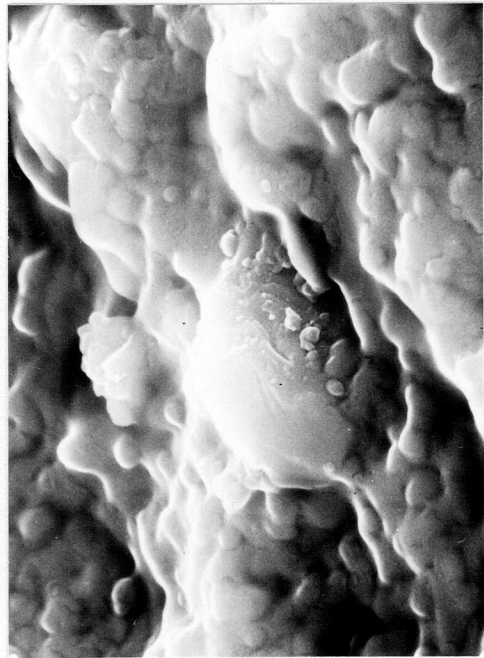at 1600°C and 3.0 GPa.

Fig. IV-5 SEM photographs of fracture surfaces of the compacts fabricated from α-Si_3N_4 powder.

Conditions; (a) compressed at 3.0 GPa and room temperature, and then sintered at 1600°C and 3.0 GPa for

(b) flash, (c) 1 min, (d) 5 min, (e) 10 min and (f) 60 min.

for α-Si_3N_4 fabricated at various pressure-temperatures for 5 minutes are indicated in Fig. IV-6. Fig. IV-6 (a) shows the perfect grain boundary fracture surface, and (b) indicates the transient state. The self-bonding and the transgranular fracture surfaces are observed in Fig. IV-6 (c), (d), (e) and (f). In particular, as illustrated in Fig. IV-6 (d), (e) and (f), the specimens which were high pressure sintered at 1800°C, show the sharp grain boundary morphology in contrast with those sintered at 1600°C.

The microstructure change during high pressure sintering of β-Si_3N_4 powder at 1600°C and 3.0 GPa is shown in Fig. IV-7. The relative densities of these specimens were already presented in Fig. IV-4. Since β-Si_3N_4 was prepared from α-Si_3N_4 by the heat treatment under nitrogen pressure, it revealed remarkable columnar grain growth probably elongated along c-axis and its average grain size was about 2 μm in diameter and 20 μm in length. The starting powder of β-Si_3N_4, which was prepared by grinding the above mentioned powder, showed the morphology of about a half size of as-grown β-Si_3N_4 particles and partially crushed down. Fig. IV-7 (a) shows the surface of the specimen compressed at 3.0 GPa and room temperature. The columnar morphology has not been distinctly observed yet. The specimens which was consolidated up to 83 - 86 % of the theoretical density, whose microstructures are shown in Fig. IV-7 (b) and (c), remain the morphology illustrated in Fig. IV-7 (a). On the contrary, initial grain morphology is not remained
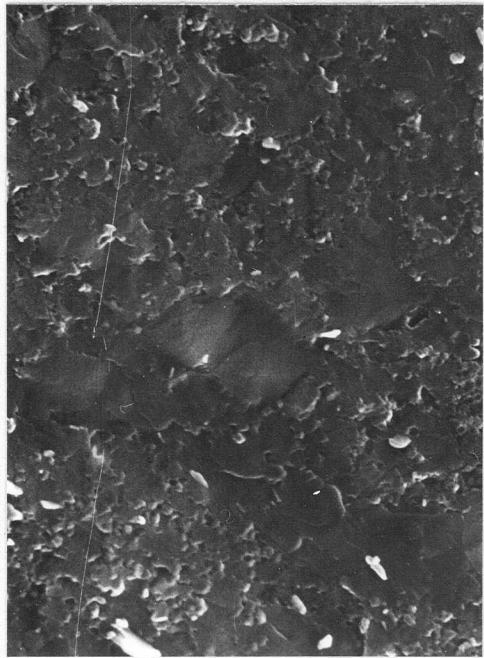
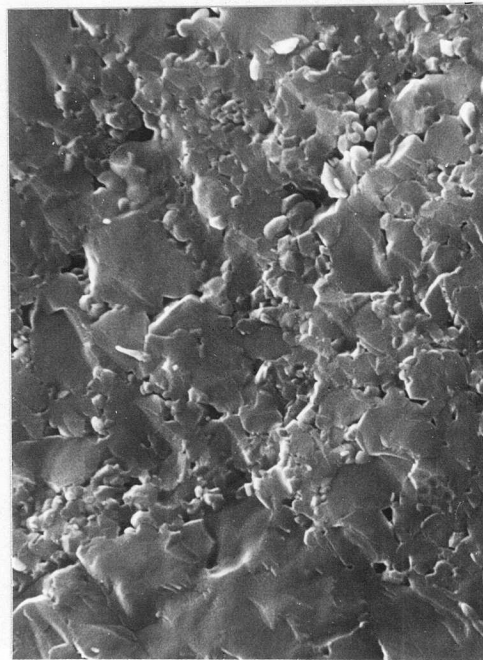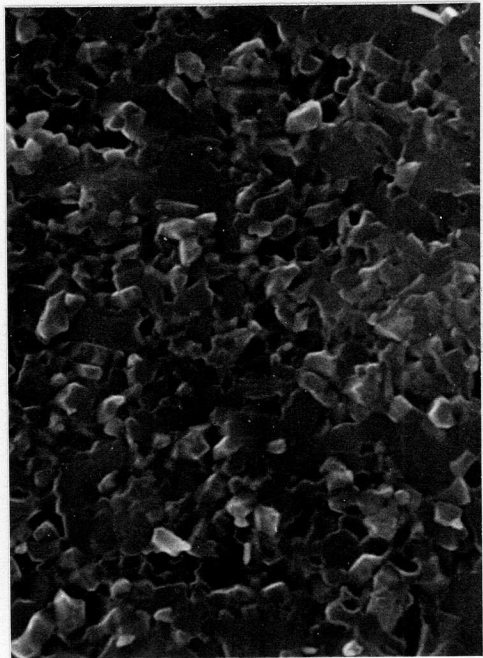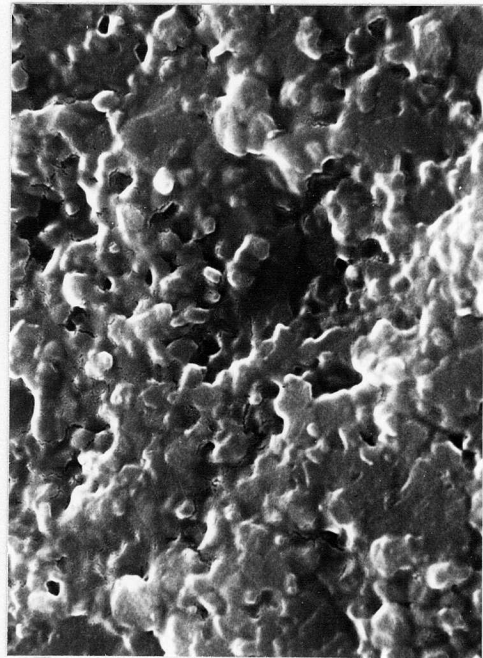Fig. IV-6   SEM photographs of fracture surfaces of the compacts sintered from α-Si$_3$N$_4$ for 5 minutes.
Conditions; (a) 1.0 GPa, 1600°C, (b) 3.0 GPa, 1600°C, (c) 5.0 GPa, 1600°C, (d) 1.0 GPa, 1800°C, (e) 3.0 GPa, 1800°C and (f) 5.0 GPa, 1800°C.
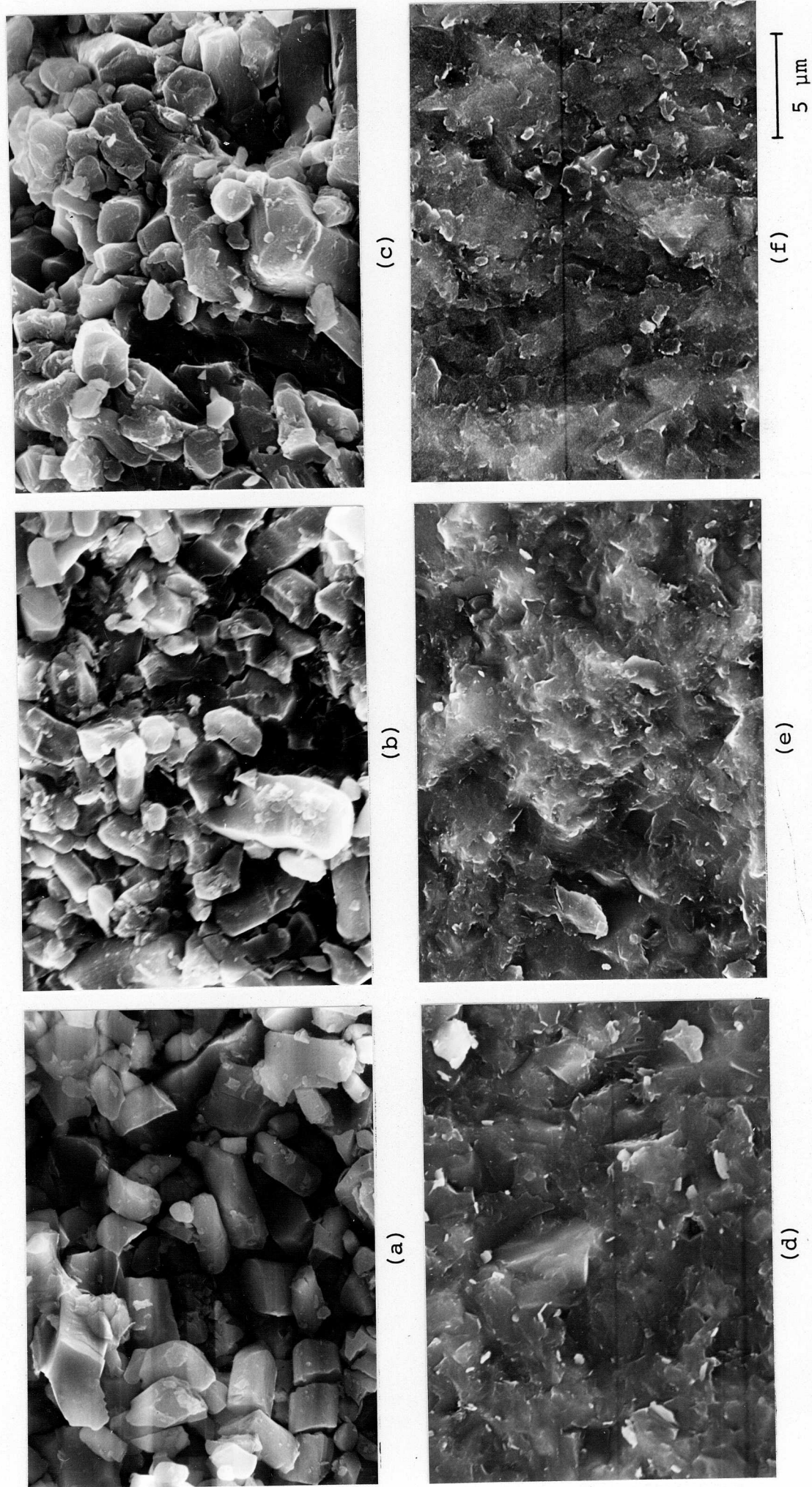
Fig. IV-7 SEM photographs of fracture surfaces of the compacts fabricated from β-Si₃N₄ powder.

Conditions; (a) compressed at 3.0 GPa and room temperature, and then sintered at 1600°C and 3.0GPa for

(b) flash, (c) 1 min, (d) 5 min, (e) 10 min and (f) 60 min.

any more in Fig. IV-7 (d), (e) and (f). For these photographs, the grains or the grain boundaries are not distinguished on the fracture surfaces.

Microhardness measurement was conducted on the pure Si_3N_4 specimens high pressure sintered at 1600°C and 3.0 GPa. Vickers microhardness (H_v) and the relative densities against the amount of β phase are shown in Fig. IV-8. When the amount of β phase is about 10 wt%, the relative density reaches almost fully theoretical one. On the other hand, microhardness gradually increases with the increase of β phase and levels off at about 22 $GN \cdot m^{-2}$ when the β phase attains about 40 wt%. And the following increase of the β phase content due to the elongation of sintering time does not develop the microhardness.

IV-3   Sintering Mechanism of Silicon Nitride in High Pressure Sintering

Fig. IV-9 shows the temperature dependence of densification of Si_3N_4 using α-Si_3N_4 as starting material. The density of the specimen gradually increases with increasing the sintering temperature, and finally reached the theoretical one at about 1600°C without having the end point density which existed in case of the fine powders of Si and TiC. In case of Si_3N_4, the mechanical strength was kept at elevated temperatures and the drastic densification caused by the brittle-ductile transition was not observed. Furthermore, since the diffusion coefficients of the constituent elements are very small,[74] it is considered that closed pores were hardly formed by
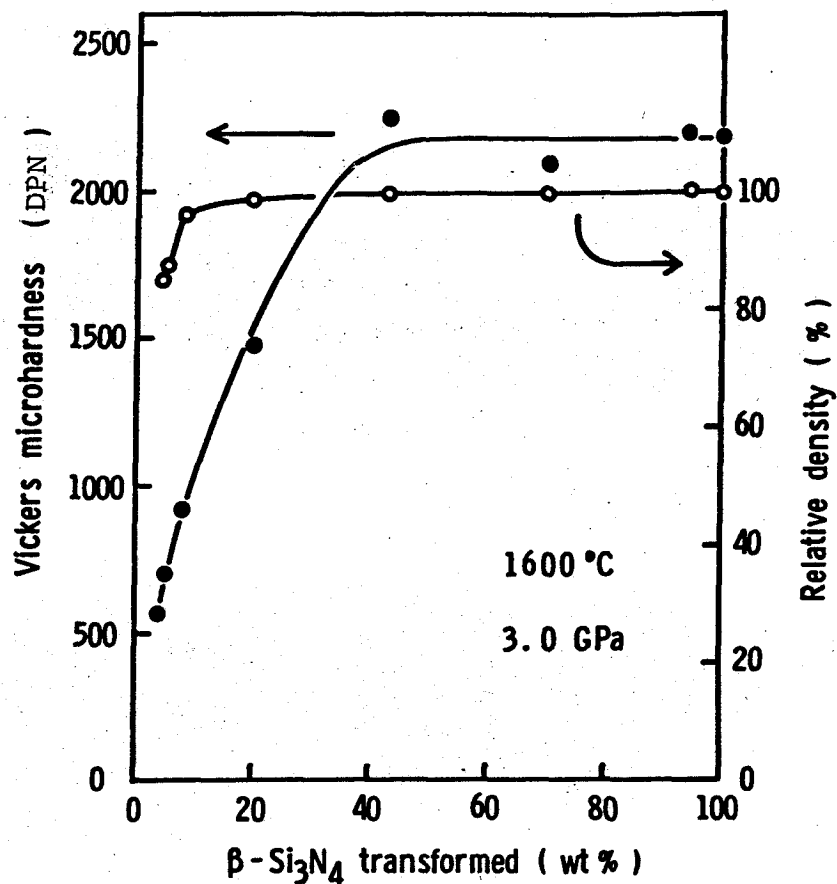
Fig. IV-8 Dependence of Vickers microhardness and relative density on the amount of transformed β-Si_3N_4 weight fractions. Specimens are the same as shown in Fig. IV-2 (a).
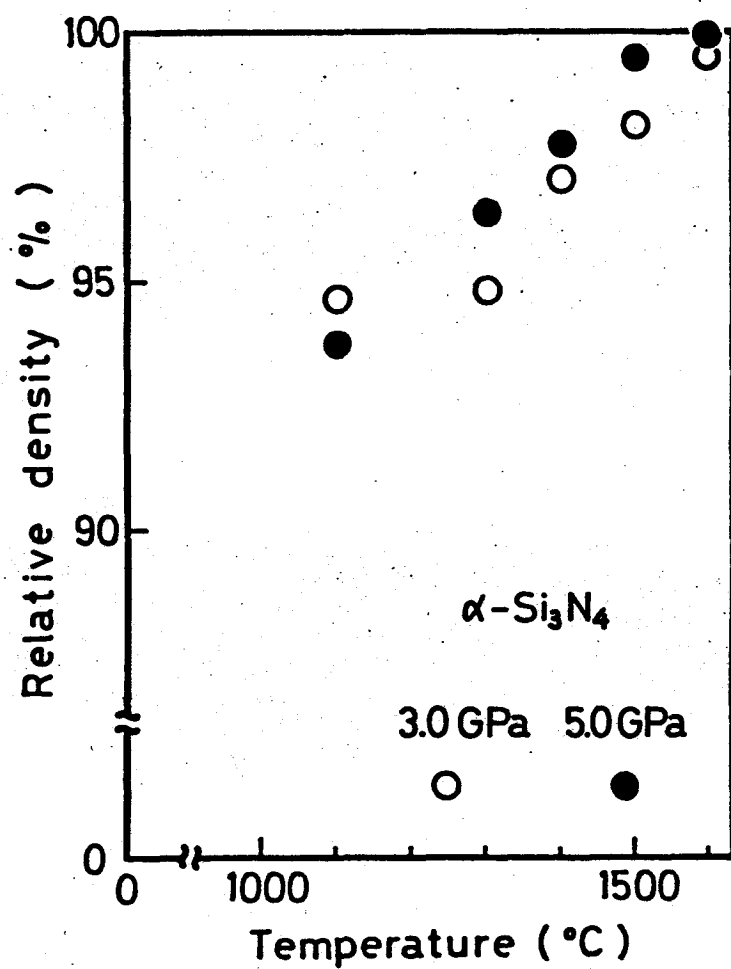
Fig. IV-9 Relative density vs temperature for Si_3N_4 sintered at 3.0 and 5.0 GPa for 30 minutes using α-Si_3N_4 as the starting material.

mass transport in a short duration of sintering. The absence of closed pores resulted the inhomogeneous application of stress on the particles, and the stress enhanced diffusion took place. So, Si_3N_4 did not have an end point density, and was densified to the theoretical density by raising the temperature.

The possible sintering mechanism of Si_3N_4 accompanied with the phase transformation is summarized in Fig. IV-10. Fragmentation and rearrangement caused by application of external pressure become dominant to the densification at the first stage. Since the ductile character of Si_3N_4 does not seem to exist, the plastic deformation hardly occurs at elevated temperatures. In the next stage, the stress enhanced diffusion becomes dominant, because the closed pores are hardly formed in the sintered Si_3N_4 specimen due to small diffusion coefficients of the constituent elements. When $\alpha-Si_3N_4$ is used as the starting powder, the phase transformation from $\alpha-$ to $\beta-$ Si_3N_4 simultaneously takes place in this stage. The phase transformation of Si_3N_4 does not contribute to the densification but develops the microhardness of the sintered specimens. Even if the theoretically dense specimen of Si_3N_4 is achieved by the stress enhanced diffusion, it must be necessary to elongate the sintering duration or to heat at higher temperatures to obtain the well self-bonded strong Si_3N_4 ceramic, considering the effect of phase transformation on the mechanical strength.

Densification Mechanism and Self-Bonding in High Pressure Sintering

Brittle region | Ductile region | Self-bonding

Fragmentation → Plastic → Stress-enhanced → Volume
Rearrangement (T) deformation | diffusion | diffusion

Open pore | Closed pore

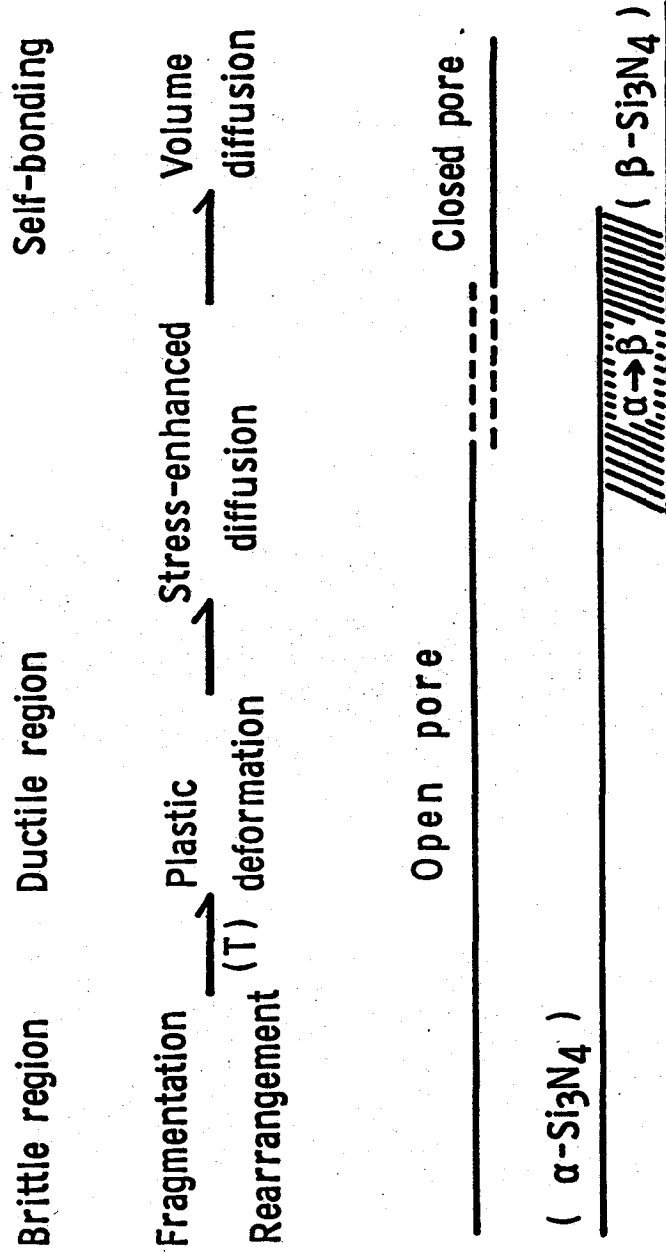(α-Si$_3$N$_4$) | ($\alpha \rightarrow \beta'$) | (β-Si$_3N_4$)

Fig. IV-10 Schematic diagram of densification mechanism and self-bonding in high pressure sintering.

Chapter V

Mechanical and Thermal Properties of High Pressure

Sintered Titanium Carbide and Silicon Nitride

V - 1   Introduction

Sintering mechanism of the pure non-oxide materials under high pressure was discussed in the previous chapter. In this chapter, the mechanical and thermal properties of pure TiC and Si_3N_4 obtained in this work are described. It is well known that these properties strictly depend on porosity, grain size and the performance of the self-bonding between grains of the material. In comparison with the results reported in literatures, the properties of the specimens fabricated by high pressure sintering are evaluated.

V - 2   Vickers Microhardness of High Pressure Sintered Titanium Carbide and Silicon Nitride

Vickers microhardness was measured as one of the mechanical properties of the sintered bodies. The indentation hardness testing is very simple and easy to measure for small specimens, and the experimental results give us an useful knowledge on mechanical properties of the high temperature structural materials. The value of Vickers microhardness is defined as the magnitude of load born on a unit area of the specimens. Microscopically it means the resistance against the plastic deformation,[75] and microscopically it is considered to be a function of

of the interatomic forces.[76] Since 1950, several empirical and theoretical relations have been proposed between hardness and yield strength of many materials.[77] Recently the fracture toughness of ceramic materials has been evaluated from the results obtained by the indentation technique.[78,79] Although these relationships between hardness and other mechanical properties are in a step of development, it is certain that the hardness testing is one of the effective methods to study the mechanical properties of the materials at elevated temperatures.

The temperature dependence of Vickers microhardness of TiC is shown in Fig. V-1, in which the present data are compared with those reported in literatures.[50] The specimen under investigation was fabricated at 5.0 GPa and 1500°C for 30 minutes using 1.3 μm TiC powder as starting material. The density of the specimen was about 96 % of the theoretical one. As seen in this figure, the present result is in good agreement with the results reported by several other investigators. Especially, the good agreement of data between the high pressure sintered body and single crystals of TiC indicates that the strong self-bonding between grains is performed in the present sintered body.

The temperature dependences of microhardness of Si_3N_4 fabricated by various conditions of the high pressure sintering are presented in Fig. V-2. In this figure, the specimen assigned as ∇ was fabricated using β-Si_3N_4 powder as the starting material, and the others were obtained from α-Si_3N_4 powders. Comparing the results
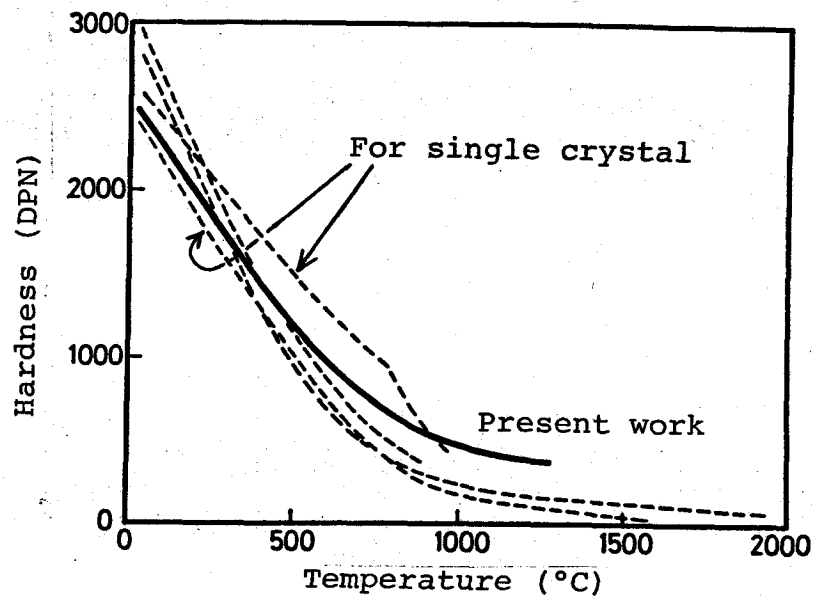
Fig. V-1 Comparison of present data of hardness
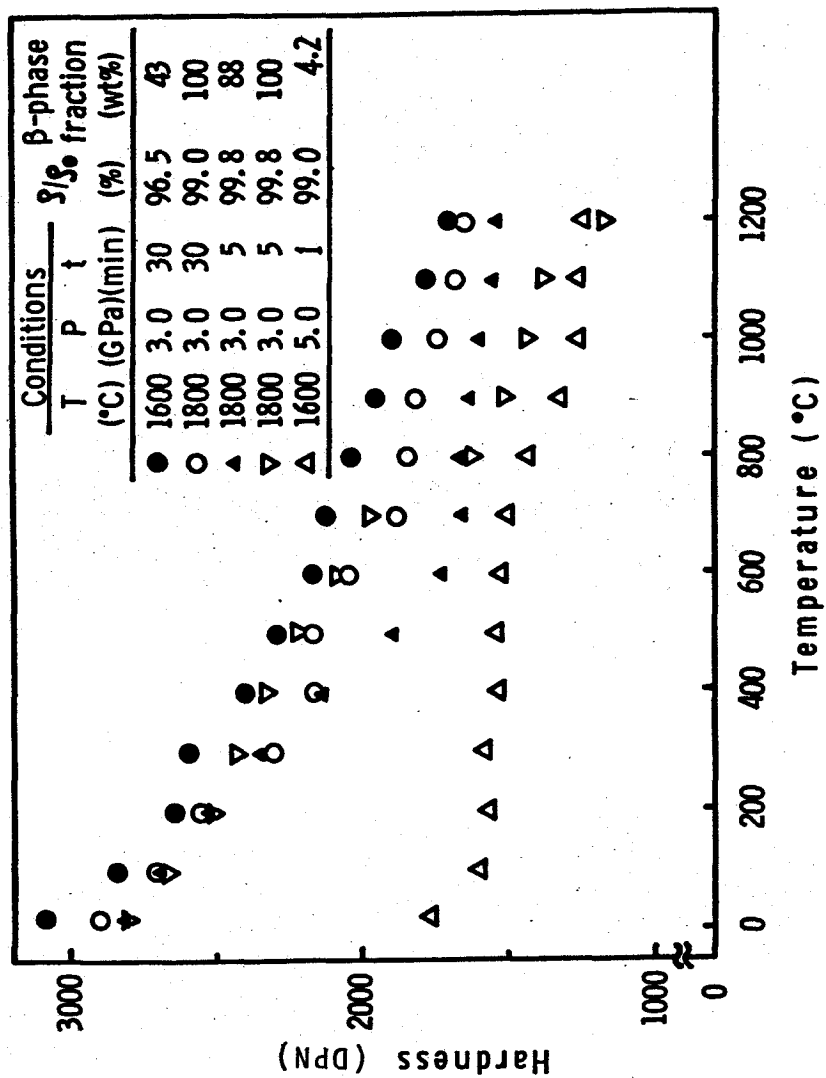for TiC with data obtained by other investigators.

Fig. V - 2 Temperature dependence of Vickers microhardness for high pressure sintered Si_3N_4 fabricated under various conditions.

obtained from α- and β-Si_3N_4, the former keeps the high hardness at elevated temperatures and the latter shows the abrupt decrease at the temperature range above 700°C. It is very interesting that the hardness of high pressure sintered specimen shows the little dependence on temperature. This behavior is quite similar to that of the reaction sintered body[80] whose bending strength generally develops at elevated temperatures. Comparing the hardness of the specimens sintered at 1600°C and at 1800°C under 3.0 GPa each other, it is clear that the sintering temperature does not affect remarkably on the hardness of the sintered bodies. Moreover, it is noteworthy that the specimen containing 43 wt% β phase exhibits the highest hardness such as 30.8 $GN \cdot m^{-2}$ at room temperature and 17 $GN \cdot m^{-2}$ at 1200°C in spite of lower relative density than the others.

Comparison of Vickers microhardness of the high pressure sintered pure Si_3N_4 with the results of those containing additive[81] is shown in Fig. V-3. Y_2O_3 and MgO are the typical additives used in the conventional hot-pressing of Si_3N_4. The specimen containing MgO shows drastic decrease of hardness above 800°C due to the second phase of $MgSiO_3$ glass precipitated at grain boundaries. In case when Y_2O_3 is added, the decrease of hardness at high temperatures is slightly improved, but above 1000°C the rapid decrease of hardness is observed. When the mechanical strength of materials drastically decreases at elevated temperatures, the material are severely inconvenient for application to the high
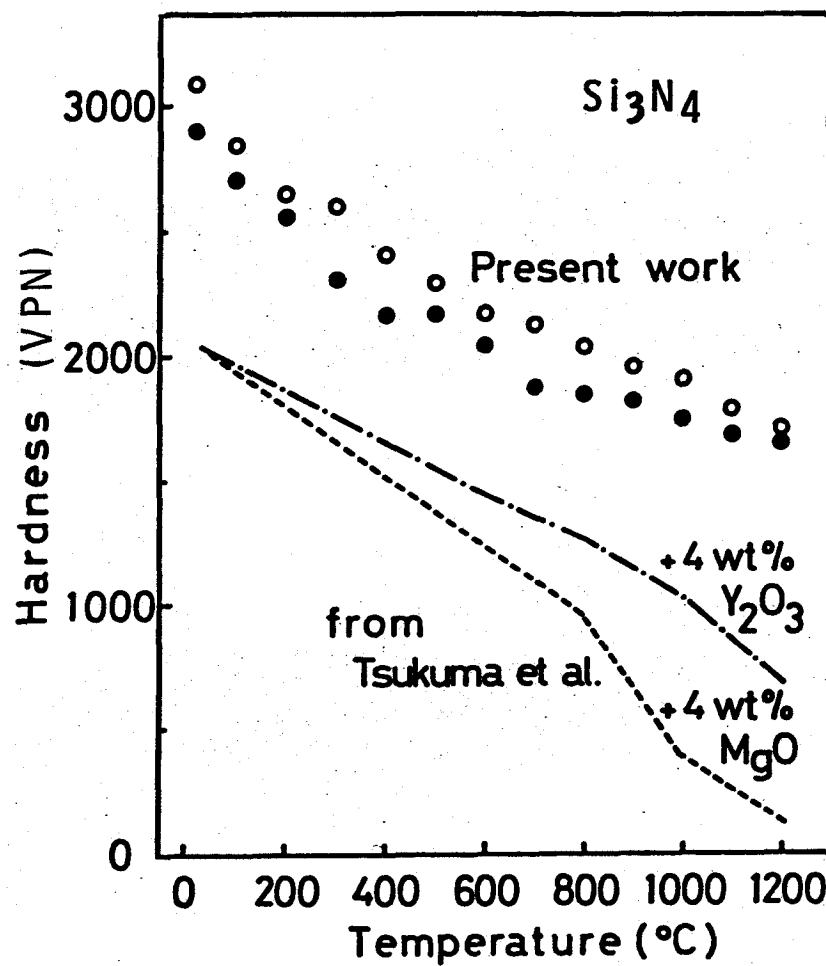
Fig. V-3 Comparison of temperature dependence of Vickers microhardness between high pressure sintered Si_3N_4 with and without additives.

temperature structural materials. However, high pressure sintered Si_3N_4 specimens without additives have high hardness values at room temperature and elevated temperatures. Besides, they do not exhibit the drastic decrease of hardness at elevated temperatures. Therefore, it is concluded that the present highly dense and pure Si_3N_4 ceramic fabricated by the high pressure sintering are suitable for the application to the high temperature structural material.

V - 3   Thermal Diffusivity of High Pressure Sintered Silicon Nitride

The properties such as small thermal expansion coefficient, large thermal conductivity and high resistance against thermal shock are required for the high temperature structural materials. Thermal conductivity is defined as the product of thermal diffusivity, specific heat and density of the material. In the present study, in order to estimate of the thermal properties of high pressure sintered Si_3N_4 bodies, the thermal diffusivity were measured by the laser pulse method. The thermal diffusivity is an inherent characteristic of the material and usually used for the estimation of thermal property. There are many investigations on the thermal properties of Si_3N_4 fabricated by various techniques[82-84] such as conventional hot-pressing with additives, reaction sintering and chemical vapor deposition.

The temperature dependence of thermal diffusivities of Si_3N_4 fabricated by various methods are presented in Fig. V-4. The present specimen was sintered at 1800°C
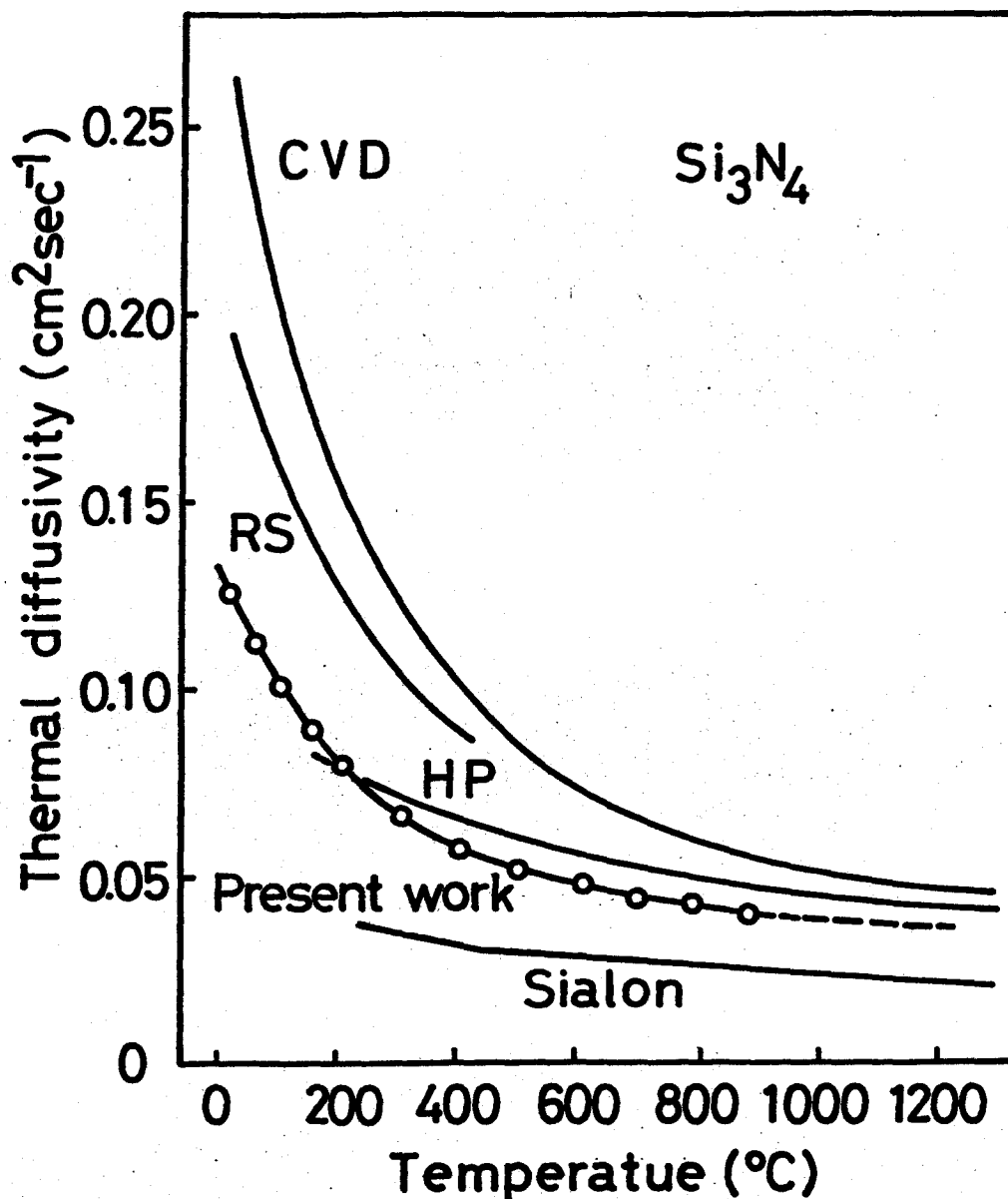
Fig. V-4 Comparison of thermal diffusivity for high pressure sintered Si_3N_4 with those obtained by others. Abbreviations such as CVD, RS, HP and Sialon indicate chemical vapor deposition, reaction sintering, hot-pressing with MgO and a compound in the Si_3N_4-Al_2O_3 system, respectively.

and 3.0 GPa for 60 minutes. Chemical vapor-deposited Si_3N_4 have the largest thermal diffusivity at all temperature range from 20°C to 1200°C. Comparing these 5 sets of thermal diffusivity data each other shown in Fig. V-4, it is considered that the thermal diffusivity is effectively influenced by the grain boundary scattering of phonon due to the lattice distortion. Considering that the grain size of high pressure sintered specimen is very small, the reason for the smaller thermal diffusivity of the present specimen than that of CVD-Si_3N_4 at room temperature is well explained by the grain boundary scattering of phonon[85]. The difference, however, becomes much smaller at elevated temperature where the operation of these high temperature materials are expected.

Summary

The present study aimed to clarify the sintering mechanism of covalent materials in high pressure sintering. Three kinds of materials such as Si, TiC and Si_3N_4 were selected for this purpose. The sintering mechanism was devided into two stages; densification stage and diffusion stage. The effect of pressure on sintering was also discussed in detail. Another purpose was to consolidate the pure non-oxide ceramics which are expected as new high temperature structural materials in near future. As a result, highly pure and dense sintered bodies could be fabricated by high pressure sintereing without any additives. The evaluation of mechanical and thermal properties of the specimens obtained in this study was also examined.

In Chapter II, the following experimental results were obtained.

1)   The densification behavior was strongly influenced by various factors such as pressure, temperature and particle size of the starting powder.

2)   The effect of pressure on densification was remarkable in the brittle region of the sintered material.

3)   The relative density increased with increasing the temperature. Especially the densification was rapidly promoted by the plastic deformation when the sintering temperature exceeded the brittle-ductile transition temperature of the material.

4) When fine powder was used as the starting material, the relative density was smaller than that of coarser powder in the brittle region due to the large friction between particles. No difference of density was observed in the ductile region.

5) An end point density was observed when fine powder was used as the starting material. It was considered to be caused by the formation of closed pores.

As a result, the following densification process was concluded; fragmentation and rearrangement of particles caused by application of pressure are dominant in the brittle region, and that, on heating, the particle rearrangement and plastic deformation become dominant to promote the densification rate.

In Chapter III, the following experimental results were obtained.

1) The temperature dependence of diffusion coefficient of carbon in TiC under quasihydrostatic pressures of 1.0 and 3.0 GPa were obtained as follows.

$$1.0 \text{ GPa} \quad D = (4.01 \times 10) \exp\left(-\frac{(3.75 \pm 0.18) \times 10^5}{R\,T}\right)$$
$$(cm^2 sec^{-1})$$
$$3.0 \text{ GPa} \quad D = (5.48 \times 10) \exp\left(-\frac{(3.83 \pm 0.25) \times 10^5}{R\,T}\right)$$

2) The diffusion coefficients of carbon in TiC were by an order of magnitude smaller under quasihydrostatic high pressure of 1.0 and 3.0 GPa than under pressureless condition in the temperature range from 1200°C to 1500°C. This result was well expalined by the mode of vacancy mechanism of diffusion under pressure.

As a result, the final stage in pressure sintering was classified into two regions such as the stress

enhanced diffusion and the retarded diffusion. The stress enhanced diffusion due to inhomogeneous distribution of stress in grains was dominant when open pores existed in the sintered body, and the stress retarded diffusion due to homogenity of stress became dominant when closed pores formed.

In Chapter IV, the following results were obtained.

1) β-Si_3N_4 was stabilized under high pressure-temperature conditions. The conversion rate of α- to β-Si_3N_4 was also accelerated by applied temperature-pressure.

2) When α-Si_3N_4 was used as the starting material, the Si_3N_4 ceramic with the theoretical density was attained even under 1.0 GPa at 1600°C by high pressure sintering for a long duration.

3) No differences in densification behaviors were found between α- and β-Si_3N_4 powders used as the starting material.

4) The fracture surfaces observed using SEM showed the existence of self-bonding between grains and the formation of polyhedrons.

5) Time dependence of both densification and phase transformation from α to β of Si_3N_4 without additives was observed in high pressure sintering.

6) No end point density was observed in high pressure sintering of Si_3N_4.

As a result, the possible sintering mechanism of Si_3N_4 was considered as follows; after the densification due to fragmentation and rearrangement of particles

caused by application of external pressure, the stress enhanced diffusion becomes dominant to densification simultaneously accompanied by α to β phase transformation.

In the last chapter, the following results were obtained.

1) The temperature dependence of Vickers microhardness of high pressure sintered pure TiC was in good agreement with that of single crystal, which indicated the strong self-bonding between grains in the sintered body.

2) High pressure sintered pure Si_3N_4 using α phase as starting powder kept higher hardness at elevated temperatures than that obtained from β phase as starting powder.

3) The drastical decrease of hardness at elevated temperatures was not observed for high pressure sintered Si_3N_4 without additives, which is always observed for hot-pressed bodies containing additives.

4) High pressure sintered pure Si_3N_4 containing 43 wt% β phase exhibited the highest hardness such as 30.8 $GN \cdot m^{-2}$ at room temperature and 17 $GN \cdot m^{-2}$ at 1200°C.

5) High pressure sintered pure Si_3N_4 had smaller thermal diffusivity than $CVD-Si_3N_4$ at room temperature reflecting the small grain size. However, the difference was much smaller at elevated temperature.

In final, it was concluded that highly pure and dense Si_3N_4 ceramic fabricated by high pressure sintering was suitable for the application to high temperature structural material.

Acknowledgement

References

1. H. B. Probst, Am. Ceram. Soc. Bull., $\underline{59}$, 206 (1980)

2. R. Naito, "Ceramic Data Book '80", No. 62, 317 (1980)

3. K. Komeya, Ceramics, $\underline{13}$, 309 (1978)

4. F. Noda, Toyota Gijutsu, $\underline{27}$, 464 (1978)

5. F. Noda, Toyota Gijutsu, $\underline{27}$, 477 (1978)

6. S. Hyodo, Ceramics, $\underline{11}$, 975 (1976)

7. W. Komatsu, T. Shimohira and Y. Moriyoshi, "Reactivity of Solids", Kagaku Sosetsu, No. 9, Gakkai Shuppan Center, p.41 and p.237 (1975)

8. Y. Moriyoshi, Gypsum & Lime, No. 152, 17 (1978)

9. J. H. Rosolowski and C. Greskovich, J. Am. Ceram. Soc., $\underline{58}$, 177 (1975)

10. B. Wong and J. A. Pask, J. Am. Ceram. Soc., $\underline{62}$, 138 (1979)

11. J. E. Blendell and R. L. Coble, Powder Mat. Inter., $\underline{10}$, 65 (1978)

12. G. De Portu and P. Vincenzini, Ceramurgia Inter., $\underline{5}$, 165 (1979)

13. G. G. Deeley, J. M. Herbert and N. C. Moore, Powder Met., $\underline{8}$, 145 (1961)

14. R. Kossowsky, J. Mat. Sci., $\underline{8}$, 1603 (1973)

15. P. Drew and M. H. Lewis, J. Mat. Sci., $\underline{9}$, 261 (1974)

16. Y. Inomata, K. Kino, T. Matsuyama and T. Wada, Yogyo-Kyokai-Shi, $\underline{84}$, 534 (1976)

17. Y. Inomata, Y. Hasegawa and T. Matsuyama, Yogyo-Kyokai-Shi, $\underline{85}$, 29 (1977)

18. L. J. Bowen, R. J. Weston, T. G. Carruthers and

R. J. Brook, "Advances in Ceramics Processing",
Ed. by P. Vincenzini, Cooperative Grafiche Galeati,
p.162 (1976)

19. G. E. Gazza, J. Am. Ceram. Soc., 56, 662 (1973)

20. George E. Gazza, Am. Ceram. Soc. Bull., 54, 778
(1975)

21. G. Q. Weaver and J. W. Lucek, Am. Ceram. Soc. Bull.,
57, 1131 (1978)

22. M. Mitomo, Yogyo-Kyokai-Shi, 85, 50 (1977)

23. R. E. Loehman and D. J. Rowciffe, J. Am. Ceram. Soc.,
63, 144 (1980)

24. D. W. Richerson, Am. Ceram. Soc. Bull., 52, 560
(1973)

25. A. Tsuge and K. Nishida, Am. Ceram. Soc. Bull., 57,
424 (1978)

26. R. Becker and F. Thummler, "Materials Science
Monographs, 6", Energy and Ceramics, Ed. by
P. Vincenzini, Elsevier Scientific Publishing
Company, p.610 (1980)

27. L. J. Bowen, T. G. Carruthers and R. J. Brook,
J. Am. Ceram. Soc., 61, 335 (1978)

28. T. Mah, K. S. Mazdiyasni and R. Ruh, J. Am. Ceram.
Soc., 62, 12 (1979)

29. F. F. Lange, Am. Ceram. Soc. Bull., 59, 239 (1980)

30. C. Greskovich and J. H. Rosolowski, J. Am. Ceram.
Soc., 59, 336 (1976)

31. F. L. Riley, Materials Science Monographs, 6, Energy
and Ceramics, Ed. by P. Vincenzini, Elsevier
scientific Publishing Company, p.550 (1980)

32. J. S. Nadeau, Am. Ceram. Soc. Bull., 52, 170 (1973)

33. S. Prochazka and W. A. Rocco, High Temp.-High Press., 10, 87 (1978)

34. M. Shimada, N. Ogawa, M. Koizumi, F. Dachille and R. Roy, Am. Ceram. Soc. Bull., 58, 519 (1979)

35. H. C. Yeh and P. F. Sikora, Am. Ceram. Soc. Bull., 58, 444 (1979)

36. J. P. Singh, A. V. Virkar, D. K. Shetty and R. S. Gordon, J. Am. Ceram. Soc., 62, 179 (1979)

37. S. D. Skrovanek and R. C. Bradt, J. Am. Ceram. Soc., 62, 215 (1979)

38. R. W. Rice, S. W. Greiman and J. J. Mecholsky, Jr., J. Am. Ceram. Soc., 63, 129 (1980)

39. F. F. Lange, J. Am. Ceram. Soc., 56, 445 (1973)

40. C. P. Gazzara and D. R. Messier, Am. Ceram. Soc. Bull., 56, 777 (1977)

41. H. C. Dunegan "Notes on Hardness Measurements of Polycrystalline Materials" Mechanical Properties of Engineering Ceramics III, Ed. by W. W. Kriegel and H. Palmour, Inter-science Publishers, New York, p.521 (1961)

42. A. R. C. Westwood, N. H. Macmillan and R. S. Kalyoncu, J. Am. Ceram. Soc., 56, 258 (1973)

43. M. V. Swain, R. M. Latanision and A. R. C. Westwood, J. Am. Ceram. Soc., 58, 372 (1975)

44. W. J. Parker, R. J. Jenkins, C. P. Butler and G. L. Abbott, J. Appl. Phys., 32, 1679 (1961)

45. E. G. Rochow, "The Chemistry of SILICON", Pergamon Press (1975)

46. S. E. Babb, Jr., Rev. Modern Phys., 35, 400 (1962)

47. J. M. Fairfield and B. J. Masters, J. Appl. Phys., 38, 3148 (1967)

48. E. Dempsey, Phil. Mag. 8, 285 (1963)

49. S. P. Denker, J. Less-Common Metals, 14, 1 (1968)

50. D. L. Kohlstedt, J. Mat. Sci., 8, 777 (1973)

51. K. Kitazawa, Yogyo-Kyokai-Shi, 83, 7 (1975)

52. C. Herring, J. Appl. Phys., 21, 437 (1950)

53. T. Vasilos and R. M. Spriggs, "Pressure Sintering of Ceramics" in Progress in Ceramic Science, vol. 4, Ed. by J. E. Burke, Pergamon Press, p.95 (1966)

54. T. Shimohira, Yogyo-Kyokai-Shi, 79, 34 (1971)

55. J. B. Hudson and R. E. Hoffman, Trans. AIME, 221, 761 (1961)

56. C. Wagner, "Diffusion in Solids, Liquids, Gases," Ed. by W. Jost, Academic Press, p.69 (1960)

57. C. A. Vansant and W. C. Phelps, Jr., Trans. ASE, 59, 105 (1966)

58. E. K. Storms, "The Titanium-Titanium Carbide System", vol. 2 of a series of monographs "Refractory Materials", Ed. by J. L. Margrave, p.1 (1968)

59. S. Sarian, J. Appl. Phys., 39, 3305 (1968)

60. O. Kamigaito, Toyota R & D Review, 12, 34 (1977)

61. T. Hirai and S. Hayashi, Ko-on-Gakkai-Shi, 5, 17 (1979)

62. C. M. B. Henderson and D. Taylor, Trans. Brit. Ceram. Soc., 74, 49 (1975)

63. Y. Inomata and Z. Inoue, Yogyo-Kyokai-Shi, 81, 441 (1973)

64. A. Tsuge, K. Nishida and M. Komatsu, J. Am. Ceram. Soc., 58, 323 (1975)

65. H. F. Priest, F. C. Burns, G. L. Priest and E. C. Skaar, J. Am. Ceram. Soc., 395 (1973)

66. S. Wild, P. Grieveson and K. H. Jack, "Special ceramics", vol.5, Ed. by P. Popper, The British Ceramic Research Association, p.385 (1970)

67. C. W. Forrest and P. Kennedy, "Special Ceramics" vol. 6, Ed. by P. Popper, p.183 (1974)

68. P. T. B. Shaffer, Acta Cryst., B25, 477 (1969)

69. S. Prochazka and R. J. Charles, Am. Ceram. Soc. Bull., 52, 885 (1973)

70. G. R. Terwilliger and F. F. Lange, J. Am. Ceram. Soc., 57, 25 (1974)

71. P. Popper and S. N. Ruddlesden, Trans. Brit. Ceram. Soc., 60, 603 (1961)

72. L. J. Bowen, R. J. Weston, T. G. Carruthers and R. J. Brook, J. Mat. Sci., 13, 341 (1978)

73. H. Knock and G. E. Gazza, CERAMURGIA Int., 6, 51 (1980)

74. K. Kijima and S. Shirasaki, J. Chem. Phys., 65, 2668 (1976)

75. D. M. Marsh, Proc. Roy. Soc. A, 279, 420 (1963)

76. J. N. Plendl and P. J. Gielisse, Phys. Rev., 125, 828 (1962)

77. A. G. Atkins and D. Tabor, Proc. Roy. Soc. A, 292, 441 (1966)

78. B. R. Lawn and D. B. Marshall, J. Am. Ceram. Soc., 62, 347 (1979)

79. A. G. Evans and T. R. Wilshaw, Acta Metall., $\underline{24}$, 939 (1976)

80. A. Giachello and P. Popper, Materials Science Monographs, 6, Energy and Ceramics, Ed. by P. Vincenzini, Elsevier Scientific Publishing Company, p.620 (1980)

81. K. Tsukuma, M. Shimada and M. Koizumi, Am. Ceram. Soc. Bull., in Press

82. F. F. Lange, H. J. Siebeneck and D. P. H. Hasselman, J. Am. Ceram. Soc., $\underline{59}$, 454 (1976)

83. T. Hirai, S. Hayashi and K. Nihara, Am. Ceram. Soc. Bull., $\underline{57}$, 1126 (1978)

84. M. Kuriyama, Y. Inomata, T. Kijima and Y. Hasegawa, Am. Ceram. Soc. Bull., $\underline{57}$, 1119 (1978)

85. W. D. Kingery and M. C. McQuarrie, J. Am. Ceram. Soc., $\underline{37}$, 67 (1954)